REVIEW

Check for updates

Colloidal synthesis of Au nanomaterials with a controlled morphology and crystal phase *via* the [Au(I)-oleylamine] complex

Gang Wang,† Chen Ma,† Long Zheng† and Ye Chen [ID] *

Colloidal gold (Au) with a fine controlled nanostructure possesses unique physicochemical properties and great potential for a variety of applications. Recently, the crystal phase emerged as an important structural factor of Au nanomaterials in addition to the intensively studied size, shape, dimension, and architecture. Intriguingly, a majority of reports on the crystal phase-controlled colloidal synthesis of Au nanomaterials are based on the [Au(I)-oleylamine] complex, where Au(I) is coordinately attached to oleylamine and then reduced to form Au nanocrystals. However, the formation mechanisms of the unusual crystal phases in these reports remain debatable. This review aims to provide a comprehensive overview of morphology- and crystal phase-controlled synthesis of Au nanomaterials which uses the [Au(I)-oleylamine] complex as the intermediate. The various proposed formation mechanisms of different morphologies and crystal phases are discussed and the uniqueness of the [Au(I)-oleylamine] interaction is highlighted. In addition, the applications of oleylamine-capped Au nanomaterials in catalysis and electronic devices are introduced. After that, perspectives are provided on the challenges and opportunities of this direction.

1. Introduction

Gold (Au) nanomaterials possess fascinating catalytic[1,2] and optical (plasmonic)[3,4] properties, endowing them with great potential in various applications including catalysis,[5,6] energy conversion,[7] electronics,[8] biosensing,[9] bioimaging[10] and photothermal therapy.[11] To improve the performances and discover new properties of Au nanomaterials, fine-controlled wet-chemical synthesis is often adopted due to its relatively low

Department of Chemistry, The Chinese University of Hong Kong, Hong Kong, China. E-mail: yechen@cuhk.edu.hk

† Equal contribution.

Dr Ye Chen is currently an Assistant Professor in the Department of Chemistry, The Chinese University of Hong Kong. She received her B. Eng. and PhD degrees (Supervisor: Prof. Hua ZHANG) in Materials Science from Nanyang Technological University (Singapore) in 2015 and 2019, respectively. Her current research interest focuses on wet-chemical synthesis of novel inorganic nanomaterials and their applications in catalysis and clean energy.

cost, simplicity and scalability.[12,13] Since the first colloidal Au synthesis by Faraday in 1857,[14] significant advances in the size- and morphology-controlled synthesis of Au nanomaterials have been witnessed.[15–19] Choosing the suitable combination of the Au precursor-surface ligand is critical in determining the achievable nanostructures. For example, adopted from the Turkevich method,[20] the citrate ion is known to act as a reducing and stabilizing agent in aqueous systems to synthesize Au nanomaterials with different morphologies.[21,22] Another landmark method developed by Brust and Schiffrin uses a simple liquid–liquid (water–toluene) reaction to synthesize thiol ligand protected Au nanoparticles (NPs) with small diameters (1–3 nm).[23] In another classic approach, Murphy's group made use of rod-like micelles formed from the preferential binding of cetyltrimethylammonium bromide on the (100) facet and developed a two-step, seed-mediated route to prepare Au nanorods (NRs) with tunable aspect ratios.[24,25] While these size- or morphology-controlled Au nanomaterials possess tunable properties[26] and a wide range of applications,[27] almost all of them crystallize in the conventional face-centered cubic (fcc) phase, which distinguishes them from those obtained in [Au(I)-oleylamine] synthetic methods.[28,29]

Oleylamine, namely *cis*-1-amino-9-octadecene, is an 18-C long aliphatic surface ligand containing one C=C bond and one amine group.[30] The roles of oleylamine in the synthesis of colloidal Au nanomaterials are unique and different from those in other colloidal systems—the presence of the [Au(I)-oleylamine] complex enables both morphology and phase controls of Au nanocrystals.[31] Reports suggest that oleylamine can act

not only as the surface ligand, but also as the reducing agent and the solvent in the colloidal synthesis.[30,32] Typically, oleylamine-capped Au nanocrystals can be synthesized by reducing a Au(III) precursor, often HAuCl$_4$, *via* the formation of the [Au(I)-oleylamine] intermediate,[33] while some reports suggest that directly using the Au(I) precursor could provide better morphology control compared to starting from the Au(III) precursor.[34,35] The interaction between Au(I) and oleylamine is believed to originate from their aurophilic interaction, leading to the formation of the [Au(I)-oleylamine] complex.[36] Then, the Au(I) is further reduced to Au(0) by either oleylamine or other reducing agents, resulting in the formation of the oleylamine-protected Au nanocrystal. Although the adsorption behavior of oleylamine on different facets of Au nanocrystals may be different,[37] reports suggest that this parameter could be adjusted to modulate the nanostructures of Au in wet-chemical synthesis.[38,39]

Recently, phase engineering of nanomaterials (PEN) emerged as an effective methodology to modulate the phase-dependent physicochemical properties of Au nanomaterials.[40]

It is worth noting that most of the reported colloidal Au nanomaterials with unconventional phases, including 4H nanoribbons (NRBs),[39] 2H and 2H/fcc nanosheets,[41,42] 4H/fcc NRs[32] and 2H/fcc nanowires (NWs)[43] were synthesized using the [Au(I)-oleylamine] complex with some variations of synthesis conditions. Nevertheless, the formation mechanisms of these Au nanocrystals with different unconventional phases still need further investigation. Therefore, it is important to understand the formation pathways of Au nanomaterials in [Au(I)-oleylamine]-based synthesis systems, to further regulate their properties and improve their application performances. It could also provide guidance to the design and synthesis of other metal nanocrystals as well as inorganic nanomaterials with controlled morphologies and phases.

In this review, we present an overview of the relevant achievements in morphology and crystal phase control of Au nanomaterials by colloidal synthesis using the [Au(I)-oleylamine] complex. Representative studies of morphology and crystal phase control of Au nanomaterials *via* the formation of the [Au(I)-oleylamine] complex are introduced. The proposed
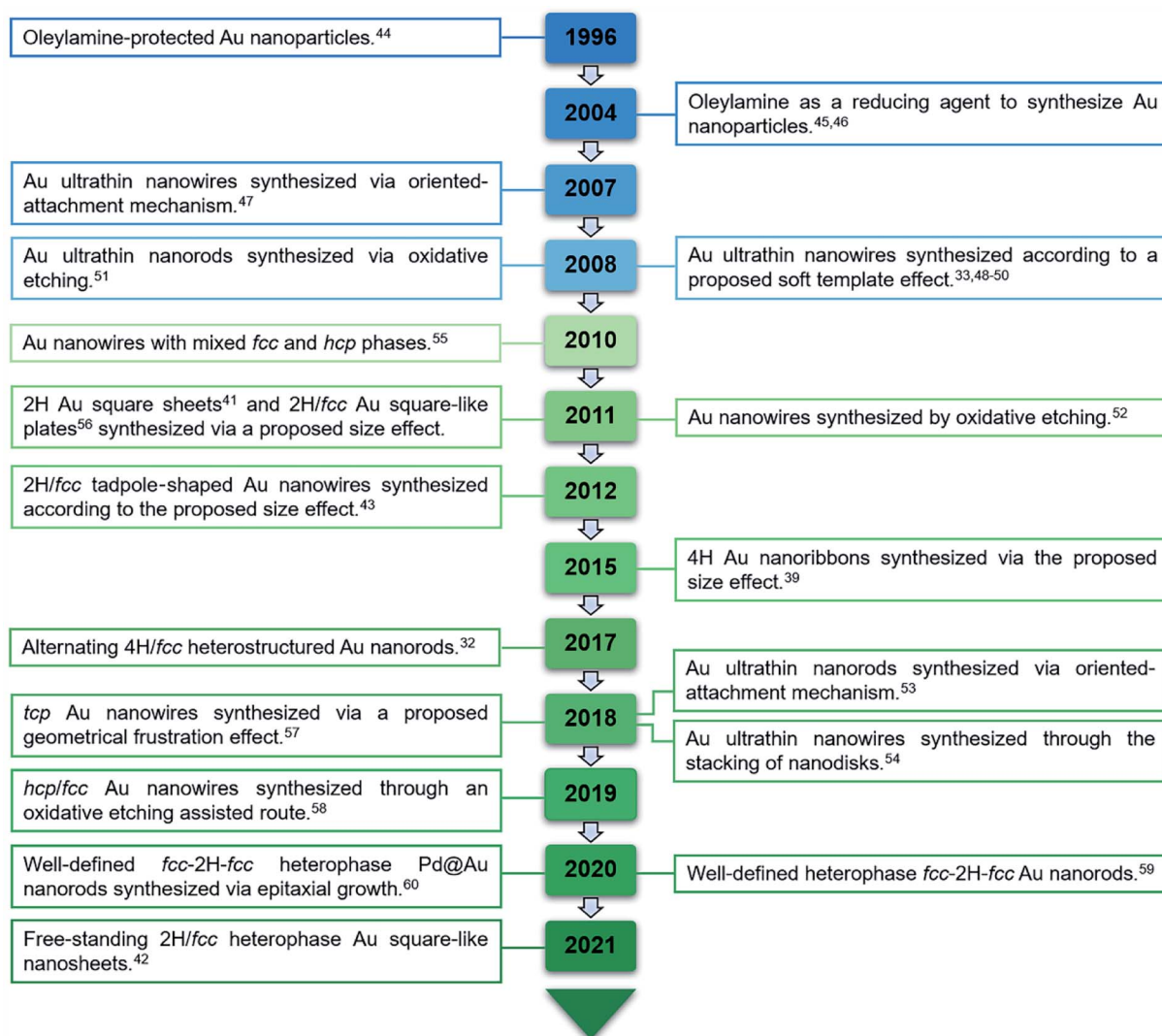

Fig. 1 Timeline showing the development of Au nanomaterials synthesized using the [Au(I)-oleylamine] complex.

This journal is © The Royal Society of Chemistry 2021

J. Mater. Chem. A, 2021, **9**, 19534–19553 | **19535**

growth mechanisms of these Au nanomaterials are discussed. After that, applications of oleylamine-capped Au nanocrystals in various catalytic reactions and electronic devices are demonstrated. Finally, some personal perspectives concerning challenges, opportunities and future research directions for this research field are presented.

2. Au nanomaterials synthesized using the [Au(ɪ)-oleylamine] complex

Fig. 1 illustrates the timeline showing some pivotal developments of Au nanomaterials synthesized using the [Au(ɪ)-oleylamine] complex. Briefly, in 1996, Leff et al. reported the synthesis of oleylamine-protected Au NPs, where oleylamine acted as the passivating ligand.[44] Then, Hiramatsu et al. and Aslam et al. investigated the role of oleylamine as a reducing agent to synthesize Au NPs in 2004.[45,46] Three years later, anisotropic single-crystalline Au ultrathin nanowires (UNWs) were synthesized by Ravishankar's group, who proposed that the Au UNWs were formed through an oriented-attachment mechanism.[47] In 2008, Yang's,[33] Xia's,[48] Sun's[49] and Giersig's[50] groups all reported the synthesis of Au UNWs under different reaction conditions. In the same year, the synthesis of Au ultrathin NRs was reported by Xia's group.[51] In 2011, Kisner et al. studied the function of oxidative etching in the synthesis of single-crystalline Au NWs.[52] In 2018, Takahata et al. reported the synthesis of Au ultrathin NRs *via* an oriented-attachment mechanism[53] and Pschunder et al. synthesized Au UNWs through the stacking of nanodisks.[54]

Notably, the above studies focused on morphology tuning of Au nanomaterials. In 2010, the Au NWs with mixed fcc and hexagonal close-packed (hcp) phases were synthesized by Kura et al.[55] Soon after that, Huang et al. made a breakthrough in crystal phase controlled synthesis of Au nanomaterials based on a proposed size effect.[41,43,56] They reported the syntheses of 2H Au square sheets (AuSSs)[41] and 2H/fcc Au square-like plates (AuSPs)[56] in 2011 and 2H/fcc tadpole-shaped Au NWs[43] in 2012. In 2015, Fan et al. reported the formation of 4H Au NRBs.[39] Two years later, the alternating 4H/fcc heterostructured Au NRs were synthesized by Chen et al. *via* one-pot wet-chemical synthesis.[32] In 2018, Vargas et al. reported the synthesis of tetrahedrally close packed (tcp) Au NWs and proposed a geometrical frustration effect.[57] Wang et al. synthesized hcp/fcc Au NWs through an oxidative etching assisted route in 2019.[58] In 2020, the well-defined heterophase fcc-2H-fcc Au and fcc-2H-fcc Pd@Au core–shell NRs were synthesized by Fan et al.[59] and Ge et al.[60] Very recently, Liu et al. reported the one-pot synthesis of free-standing 2H/fcc heterophase Au square-like nanosheets.[42]

Table 1 lists a summary of Au nanomaterials introduced in this review, including the morphology, phase, reactants (except oleylamine and Au the precursor), reaction temperature and time, and proposed growth mechanism.

2.1 Morphology control of Au nanomaterials

In this section, the Au nanomaterials with different morphologies obtained *via* the [Au(ɪ)-oleylamine] intermediate, including NPs, NWs and NRs, as well as their formation mechanisms are discussed.

2.1.1 Au nanoparticles. Earlier studies focused on the role of oleylamine in the synthesis of Au NPs. Oleylamine was first recognized as a passivating ligand by Leff et al. when they prepared the amine-protected Au NPs in 1996.[44] They found that oleylamine could form a weak covalent bond with Au atoms to stabilize the surface of Au NPs in an organic solvent. Then, the role of oleylamine as a reducing agent in preparing Au NPs was studied in 2004 in both organic[45] and aqueous[46] systems. Hiramatsu et al. synthesized Au NPs by using oleylamine as a reducing agent and surfactant at a high temperature ($\sim$110 °C) in the presence of toluene solvent.[45] They proposed that the reducing equivalents in the reaction were provided by the amino group of oleylamine, which could experience Au-ion-induced oxidation to nitriles.[61] Aslam et al. reported the preparation of oleylamine-reduced Au NPs in a mixed solution of water and oleylamine below 80 °C.[46] Interestingly although oleylamine could not dissolve in water at room temperature, water-dispersible Au NPs could be obtained at 80 °C, resulting from the thermal decomposition of the Au-oleylamine complex. Subsequently, Liu et al. used the protocol reported by Aslam et al. to further study the growth mechanism of oleylamine-stabilized Au NP growth.[62] The authors found out that the oleylamine ligands could be converted into oleylamide when Au(ɪɪɪ) species were reduced to Au(ɪ) or Au(0). Then, the oleylamide ligands generated a hydrogen-bonding network around the Au NPs. Upon heating, oleylamine or oleylamide-Au complexes were decomposed, resulting in the formation of tiny NPs ($\sim$1–3 nm), which were then recombined to form more thermally stable and larger NPs ($\sim$10 nm). Different from the above-mentioned work that used $HAuCl_4$ as the Au precursor, Lu et al. prepared Au NPs by choosing AuCl as the precursor and heating the mixture of AuCl, oleylamine and chloroform at 60 °C.[63] The Fourier Transform Infrared, mass and UV/Vis absorption spectra confirmed the initial formation of the [Au(ɪ)Cl-oleylamine] complex, which was not stable and gradually decomposed to generate element Au(0) and dioleylamine upon heating. The authors found *via* control experiments that the ability of oleylamine to control the morphology was attributed to not only the amine group but also the C=C bond, which could enhance the coordination of oleylamine with AuCl.[64]

Specific morphology controls over Au NPs, including size control, twin defect control and shape control, in the [Au(ɪ)-oleylamine] system have been achieved by varying the reaction parameters. For instance, Shen et al. proposed that when oleylamine was used as the reducing agent and surfactant, increasing the reaction temperature could increase the reduction rate of Au(ɪɪɪ) and accelerate the growth process, leading to larger size NPs (Fig. 2a).[65] By tuning the concentration of the Au precursor in oleylamine, 4-*tert*-butyl toluene and 1,2-hexadecanediol, Zhang et al. successfully synthesized single-crystalline Au NPs, decahedral multiply twinned particles (MTPs) and icosahedral MTPs at low, intermediate, and high concentrations, respectively (Fig. 2b).[66] The authors proposed that the deposition rate of Au atoms onto the particle surface could be varied by different Au precursor concentrations,

19536 | *J. Mater. Chem. A*, 2021, **9**, 19534–19553

This journal is © The Royal Society of Chemistry 2021

Table 1 Summary of Au nanomaterials synthesized using the [Au(I)-oleylamine] complex

Morphology	Phase	Reactants except oleylamine and Au precursor	Temperature and time	Proposed growth mechanism	Ref.
Nanoparticle	fcc	Water/toluene	RT[a], ~12 h	—	44
	—	Toluene	110 °C, 2 h	—	45
	fcc	Water	80 °C, —	Decomposition of [Au-oleylamine] complex	46
	fcc	Water	80 °C, 3 h	Decomposition of [Au-oleylamine] complex	62
	—	Chloroform	60 °C, 24 h	Decomposition of [Au-oleylamine] complex	63
	fcc	Toluene	65 °C, 6 h	—	65
	fcc	4-Tert-butyl toluene/1,2-hexadecanediol	200 °C, 1.5 h	—	66
	fcc	Oleic acid	Microwave, 1 min	—	38
Nanowire	—	Oleic acid/toluene/ascorbic acid	Step 1: 120 °C, step 2: RT, step 3: RT, several hours to a few days	Oriented-attachment mechanism	47
	—	—	RT, 4 days	Micellar formation mechanism	33
	—	Hexane/Ag nanoparticles	60 °C, 24–100 h	Micellar formation mechanism	48
	fcc	Route 1: oleic acid/hexane Route 2: hexane	80 °C, ~5 h	Micellar formation mechanism	49
	fcc	Chloroform	Step1: RT, 24 h Step2: 35–40 °C, several days	Micellar formation mechanism	50
	fcc	Hexane/TIPS[b]	RT, 4–5 h	Oriented-attachment mechanism	67
	—	Chloroform/CO	60 °C, 10 min	—	68
	fcc	Hexane/O$_2$	Step 1: RT, 24 h Step 2: 80 °C, 6 h	Etching mechanism	52
	fcc	—	80 °C, 24 h	Micellar formation mechanism	69
	—	—	75 °C, 5–6 h	—	71
	—	Hexane/TIPS	40 °C, 24 h	Micellar formation mechanism	72
	—	Route 1: hexane	Route 1 – step 1: 25 °C, 48 h; step 2: 45 °C, 48 h	Micellar formation mechanism	73
		Route 2: hexane/TIPS	Route 2 – 40 °C, 3 h		
	—	Hexane/TIPS	RT, 12 h	Disk stacking mechanism	54
	2H/fcc	Hexane/graphene oxide sheets	55 °C, 36 h	Size effect	43
	2H/fcc	Hexane/graphene oxide sheets	Step 1: 55 °C, 10 h Step 2: RT, 2 days	Size effect	
	hcp/fcc	—	Step 1: 60 °C, step 2: 85 °C, 2 h	Stacking fault	55
	hcp/fcc	—	65 °C, 72 h	Stacking fault	94
	hcp/fcc	CuCl$_2$	160 °C, 4 min	Oxidative etching	58
	tcp	Hexane/TIPS	RT, ~5 h	Geometrical frustration effect	57
Nanorod	fcc	Chloroform/amorphous Fe nanoparticles	RT, 6–8 days	Etching mechanism	51
	—	Cyclohexane/TIPS	Step 1: RT, 2 h Step 2: RT, 6–30 h	—	75
	—	Cyclohexane/TIPS	Step 1: RT, 2 h Step 2: RT, 30 h	Oriented attachment mechanism	53
	4H/fcc	—	70 °C, 17 h	Size effect/stacking fault	32
	fcc-2H-fcc	*n*-Dodecylamine/O$_2$	65 °C, 17 h	Oxidative etching	59
	fcc-2H-fcc	Hexane/2H-Pd nanoparticles	60 °C, 12 h	Epitaxial growth	60
Nanosheet	2H	Hexane/ethanol/graphene oxide sheets	55 °C, 16 h	Size effect	41
	2H/fcc	Hexane/ethanol/graphene oxide sheets	55 °C, 28 h	Size effect	
	2H/fcc	Hexane/ethanol/graphene oxide sheets	Step 1: 58 °C, 14 h Step 2: 58 °C, 10 h	Size effect	56
	2H/fcc	Hexane/squalene	58 °C, 17 h	Size effect	42
Nanoribbon	4H	Hexane/1,2-dichloropropane	58 °C, 16 h	Size effect	39

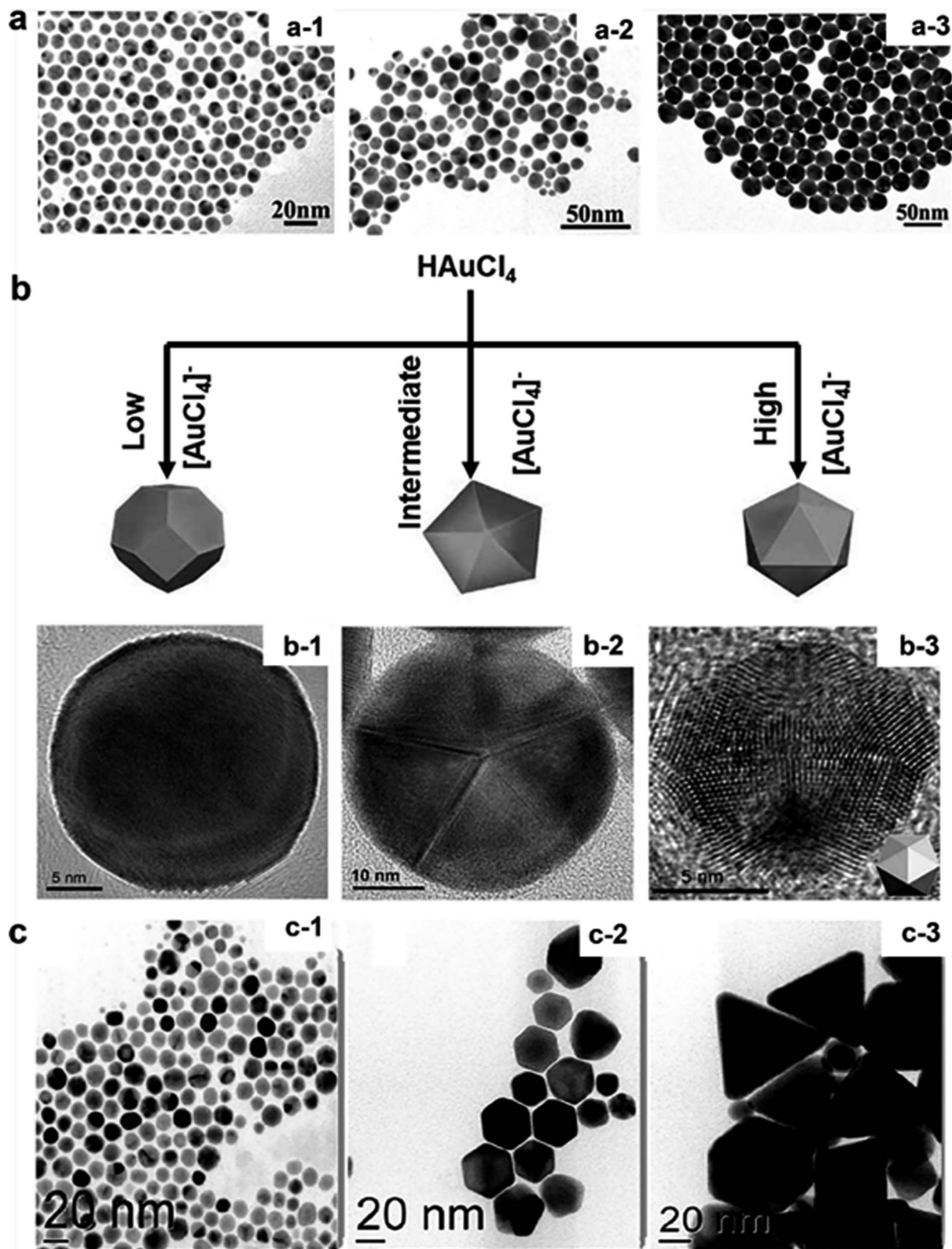[a] RT: room temperature. [b] TIPS: triisopropylsilane.

Fig. 2   (a) Transmission electron microscope (TEM) images of Au nanoparticles (NPs) prepared at different temperatures: (a-1) 75 °C; (a-2) 95 °C; and (a-3) 115 °C. Reproduced with permission.[65] Copyright 2008, American Chemical Society. (b) Crystallinity tunable synthesis of Au NP nanoparticles. (b-1) High resolution TEM (HRTEM) images of single-crystalline Au NPs; (b-2) round decahedral Au multiply twinned particle; (b-3) icosahedral Au multiply twinned particle. Reproduced with permission.[66] Copyright 2010, Wiley-VCH. (c) TEM images of Au NPs formed using (c-1) dioleamide only, (c-2) a 1 : 1 molar ratio of dioleamide and oleic acid, and (c-3) a 1 : 2 molar ratio of dioleamide and oleic acid. Reproduced with permission.[38] Copyright 2010, American Chemical Society.

leading to the formation of distinctive nanostructures. In another work, a microwave irradiation protocol was developed by Mohamed *et al.* to synthesize shape-controlled Au NPs capped with a ligand mixture of oleylamine and oleic acid.[38] The infrared (IR) spectrum result showed that in the presence of Au NPs, oleylamine could react with an equal amount of oleic acid to form dioleamide, which acted as the reducing agent and capping agent to form isotropic-shape Au NPs (Fig. 2c). When an excessive amount of oleic acid was used (oleic acid : oleylamine molar ratio $\geq$ 2 : 1), anisotropic shapes (*i.e.*, hexagons, truncated prisms and prisms) of Au NPs were obtained.

It is worth pointing out that in the early reports, the formation of oleylamine-capped Au NPs is a result of the thermal decomposition of the Au-oleylamine complex, and therefore most colloidal Au nanostructures are limited to zero dimensions.

2.1.2 Au nanowires.

Using oleylamine to prepare anisotropic Au nanocrystals with a high aspect ratio, *i.e.*, one-dimensional (1D) Au materials, was first reported by Ravishankar's group in 2007. In their work, single-crystalline Au UNWs were synthesized by using a multistep method (Fig. 3a).[47] By aging a mixture of the Au NP-oleylamine complex and ascorbic acid, bundles of Au UNWs with a diameter of ~2 nm and microscale lengths were obtained. The authors proposed an oriented-attachment mechanism, in which the presence of ascorbic acid and oleylamine aided the smoothing of attached Au NPs to form 1D structures along the $\langle 111 \rangle$ direction. In 2008, the synthesis of Au UNWs was reported by Yang's,[33] Xia's,[48] Sun's,[49] and Giersig's[50] groups based on the [Au(I)-oleylamine] system. Different from the multistep method reported by Ravishankar's group, Yang's group obtained high-yield Au UNWs (~1.6 nm in diameter) by directly aging a mixture of $HAuCl_4$ and
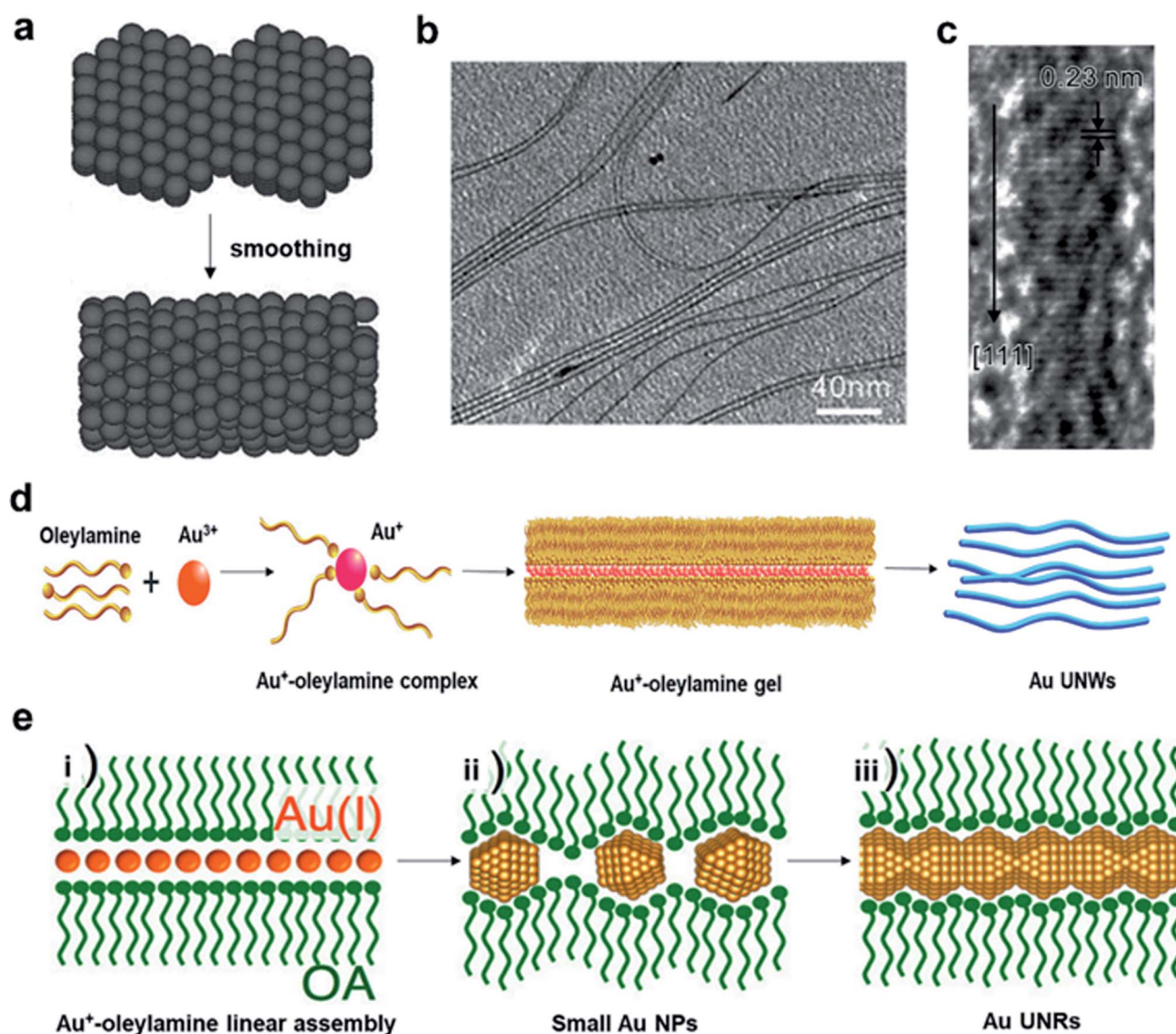

Fig. 3 (a) Schematic illustration of Au ultrathin nanowires (UNWs) with an oriented-attachment mechanism. Reproduced with permission.[47] Copyright 2007, Wiley-VCH. (b) TEM, (c) HRTEM images of Au UNWs along the $\langle 111 \rangle$ direction and (d) schematic illustration of the Au UNWs with the micellar formation mechanism. Reproduced with permission.[33] Copyright 2008, American Chemical Society. (e) Formation process of Au ultrathin nanorods with an oriented-attachment mechanism. Reproduced with permission.[53] Copyright 2018, American Chemical Society.

oleylamine for several days at room temperature (Fig. 3b).[33] The authors suggested that oleylamine served as the surfactant, reductant and solvent during the synthesis. Specifically, Au(III) was first reduced to Au(I) by the amino group of oleylamine (Fig. 3d). Then, Au(I) was further complexed with oleylamine to form a Au(I)–amine gel with long-range ordered mesostructures by the aurophilic interaction, which served as a confined high-aspect-ratio template for reducing Au(I) species to Au(0), leading to the formation of Au UNWs along this thermodynamically favored [111] growth direction (Fig. 3c). A similar soft template effect was also reported by Xia's group, who confirmed the existence of Au(I)Cl-oleylamine complex chains through [1]hydrogen-nuclear magnetic resonance (^{1}H-NMR), mass spectra, and low-angle X-ray diffraction (XRD).[48] They also found that introducing Ag NPs in the mixture of poly[Au(I)Cl-oleylamine] could lead to the favored formation of 1D structures and increase the yield of Au NWs from 20% to 70%. In the work by Sun's group, single crystalline Au NWs were synthesized with tunable diameters of 3 nm and 9 nm in the absence and presence of oleic acid, respectively.[49] The 3 nm Au NWs were prepared when oleylamine was used as the only solvent, while the 9 nm Au NWs were synthesized by mixing oleylamine and oleic acid with the volume ratio of 1 : 1. They proposed that a 1D micellar structure was first generated by the self-assembly of oleylamine–oleylamine or oleylamine–oleic acid. Then the gradual growth of small Au crystals was confined in the micelles due to the binding between the –NH_2 group of oleylamine and Au, further inducing the 1D growth of Au. In the work by Giersig's group, Au UNWs with different lengths ranging from ~10 nm to ~4 μm were obtained by adjusting the concentration of $HAuCl_4$, the reaction time and addition of the second solvent.[50] Similar to Sun's group, they proposed that the growth of Au NWs was related to elongated reverse micelles formed by the self-organization of oleylamine, followed by the reduction of Au ions inside the preformed micelles.

Besides the aforementioned studies, other studies also made some important improvements to the controlled synthesis of Au UNWs. For example, Feng et al. reported a fast method to prepare Au UNWs by using oleylamine as the shape-direct reagent and triisopropylsilane (TIPS) as an effective reductant at room temperature in 2009.[67] The reaction time was decreased from several days to 4–5 hours by introducing TIPS. Besides the TIPS, carbon monoxide (CO) was also used as a strong reducing agent to synthesize Au NWs in the [Au(I)-oleylamine] system.[68] The reaction time could be reduced to 10 minutes after adding CO. The finally obtained Au NWs with ~2.5 nm width and several micrometer lengths possessed enlarged spherical heads. A similar shape of NWs was also reported by Feng et al.[67] In addition to the effect of different reducing agents, the function of oxidative etching on the formation of single-crystalline Au NWs was also studied. Kisner et al. found that the oxygen (O_2) absorbed in the oleylamine solution could improve the yield and length of the NWs.[52] The presence of an oxidant, like O_2, was believed to enhance the oxidative etching of twin defects on the initially formed Au NPs to Au(I) or Au(III) ions, which could then be reduced and re-deposited onto the Au NPs along the axial direction with the assistance of oleylamine to form

elongated and defect-free Au NWs. Besides single-crystalline NWs, defective crystalline NWs have also been reported. Sun's group obtained bending Au NWs based on their previous work.[49,69] In this work, they applied mechanical stirring to disrupt the 1D nanocrystal formation, resulting in bending NWs with various types of crystal defects. They deduced that the formation of abundant crystal defects was related to the rather low energies of stacking faults of the Au fcc crystal[70] and the reshuffling of surface ligands caused by mechanical disturbance. Bernardi et al. prepared nanotwinned Au NWs with a high density of twin-plane defects along the [111] axis.[71] They hypothesized that the rearrangement and relaxation of bulky and asymmetric oleylamine molecules favored the formation of twinned structures.

To obtain a deeper understanding of the growth processes of Au NWs, a number of advanced characterization methods and theoretical calculations have been performed. For instance, Loubat et al. carried out in situ small-angle X-ray scattering (SAXS) to study the formation mechanism of Au NWs in the solution where $HAuCl_4$ was dissolved in hexane in the presence of oleylamine and TIPS.[72] The result showed that hexagonal superlattices were formed in the solution with a spacing of ~9.7 nm, which was likely due to a parallel assembly of Au NWs coated with an oleylamine/oleylammonium bilayer. In addition, the increase of the volume fraction of NWs, calculated from the SAXS modelling, would not reduce that of NPs, further indicating a micellar formation mechanism of the Au NWs rather than the oriented attachment of NPs. Subsequently, they further studied the growth mechanism by comparing the NW yields in different synthesis methods using in situ SAXS analysis, which could precisely determine the volume fraction of the different products in solution.[73] A large yield of 75% for NWs was achieved using the TIPS method,[67] much higher than that obtained in the synthesis using only oleylamine and $HAuCl_4$,[33] indicating that the generation of Au NWs might not follow the route via forming the [Au(I)Cl-oleylamine] soft template. The authors further proposed that the growth of Au NWs might take place in the preformed micelles of oleylamine[50] or was attributed to a cooperative effect from the oleylammonium chloride ion pair organization and Au ion reduction. Density functional theory (DFT) calculations further demonstrated that cooperative adsorption and organization of methylammonium chloride ion pairs could stabilize the surface of Au UNWs, which is similar to the "zip" mechanism[74] for the formation of Au NRs. In another theoretical investigation, You et al. used DFT calculations to investigate the mechanism invoked by Yang's group[33] via analyzing the correlation between the surface energy and adsorption energy of the oleylamine–oleylamine and oleylamine–Au.[37] The result demonstrated that the formation of micellar mesostructures was due to the strong interactions formed between the long carbon-chains of oleylamine, which prevented the diffusion of Au atoms and ions through them, promoting the formation of Au nanocrystals along with certain orientation. In addition, oleylamine preferentially adsorbs on the Au (100) facets rather than the (111) surfaces due to a stronger interaction between the amine group with the Au (100) facets, further promoting the anisotropic growth of 1D

nanowires. Pschunder *et al.* proposed a new possible formation mechanism of Au UNWs by combining *in situ* X-ray absorption fine structure spectroscopy (EXAFS) and SAXS studies.[54] A multistage growth route was introduced by the authors. Disk-shaped units were formed by complexing oleylamine with Au(III) first, followed by partial reduction of Au(III) to Au(I). Then, these units self-organized to generate cylindrical stacks, which subsequently grew into longer species with decreased diameters by reducing Au(I) to Au(0) and expelling out ligands. Finally, Au UNWs were formed with a diameter of ∼1.7 nm and assembled in a hexagonal arrangement due to the formation of a bilayer of oleylamine adsorbed on the surface of UNWs.

In brief summary, there are many possible mechanisms for the formation of Au UNWs based on the [Au(I)-oleylamine] complex: (i) the oriented-attachment mechanism by small-size Au NPs; (ii) the micellar formation mechanism, in which Au(I) combines oleylamine to form [Au(I)-oleylamine] complexes and further forms Au NWs by reducing Au(I) to Au(0), or oleylamine self-assembles into reverse micelles and induces the gradual formation of Au crystals; (iii) the etching mechanism, in which etching and redeposition of Au NPs with twin defects lead to the formation of NWs; (iv) the disk stacking mechanism, in which stacked Au nanodisks formed by complexing oleylamine with Au(III) shrink to 1D structures with the gradual reduction of Au(III) → Au(I) → Au(0).

2.1.3 Au nanorods. Au NRs are another representative kind of 1D Au nanostructure with lower aspect ratios (typically 5–50).[51,75] The synthesis of Au ultrathin NRs with a diameter of ∼2 nm and aspect ratio ∼30 was reported by Xia's group in 2008 by reducing [Au(I)Cl-oleylamine] with the presence of amorphous Fe NPs in chloroform.[51] The authors proposed that introducing amorphous Fe NPs as a reducing agent could contribute to the formation of Au NPs with abundant defects. Since the defective structures are susceptible to oxidative etching,[76] these Au NPs were unstable and would be etched by Fe(III) species and oxidized to Au(I) or Au(III). Then, the Au ions were reduced again to Au atoms and re-deposited onto the defect-free regions of Au NPs to form Au ultrathin NRs, similar to the etching effect by O_2.[52]

Another mechanism was proposed by Takahata *et al.*, who used TIPS as the reductant to prepare Au ultrathin NRs.[53,75,77] They achieved the length control of Au UNWs or ultrathin NRs with similar diameters by adjusting the concentrations of $HAuCl_4$, oleylamine, cyclohexane and TIPS.[75] Subsequently, they found that the as-prepared Au ultrathin NRs would gradually evolve into NPs when stored in chloroform in the absence of oleylamine, indicating that oleylamine plays a crucial role as a surfactant in maintaining the morphology of Au ultrathin NRs by inhibiting the diffusion of Au surface atoms.[77] Recently, they further carried out spectroscopic methods to study the growth mechanism of Au ultrathin NRs.[53] Time-resolved Au L_3-edge X-ray absorption near-edge structure spectra showed that Au(III) ions were reduced to Au(I) by oleylamine at the first stage. The Au(I) ions might further combine with oleylamine to form a 1D assembly by aurophilic interactions[48] (Fig. 3e). Then, the gradually increased absorbance only in the visible region was observed *via* time-resolved UV-vis-near-IR spectroscopy,

indicating the reduction of Au(I) to Au(0) by TIPS and the subsequent formation of small size Au NPs (<2 nm). With the increase of the reaction time, a new band with monotonously red-shifted peak position and enhanced intensity appeared in the spectra, indicating that the NPs were attached sequentially to generate Au ultrathin NRs in the oleylamine micelle. This growth route is similar to the oriented attachment mechanism introduced in Section 2.1.2.

According to these studies, the growth mechanisms of Au ultrathin NRs may follow two kinds of routes: (i) Au NPs with a high density of defects undergo an oxidation etching and redeposition process to transform into Au ultrathin NRs; (ii) Au NPs undergo an oriented-attachment mechanism in the pre-formed oleylamine micelle.

To briefly summarize Section 2.1, Au nanomaterials with different 0D and 1D morphologies have been obtained in the [Au(I)-oleylamine] system and the proposed growth mechanisms of Au NPs, UNWs and ultrathin NRs are diverse. According to the aforementioned research, the reaction parameters, including the temperature, time, substrate concentration, oxidation etching, solvents and reducing agents, play important roles in modifying the shapes, sizes and dimension of the final products.

2.2 Crystal phase control of Au nanomaterials

To date, colloidal synthesis has become one of the most effective methods to prepare Au nanomaterials with unconventional phases, leading to great progress in boosting their physico-chemical properties.[31] Fig. 4 demonstrates the schematic atomic models, corresponding high-resolution transmission electron microscopy (HRTEM) images and selected area electron diffraction (SAED) patterns of different phases and heterophase structures of Au nanomaterials synthesized *via* the [Au(I)-oleylamine] complex. Normally, Au nanomaterials crystallize in the highly symmetric fcc phase (Fig. 4a), same as their bulk counterpart. The fcc phase is their thermodynamically stable phase, which possesses a representative "ABC" stacking arrangement along the $\langle 111 \rangle_f$ close-packed directions. Although some theoretical calculations suggested that the stability of different crystal phases of Au nanomaterials (under ideal assumptions like full relaxation of atomic positions) is in the order of fcc > 4H > 2H,[78,79] the stabilization of different unconventional phases, *i.e.*, the 2H phase,[33] 4H phase[32] and heterophase[59] in Au nanomaterials has been achieved *via* the [Au(I)-oleylamine]-complex-based synthesis. Similar to the fcc phase, both 2H and 4H adopt close-packed structures, but their close-packed planes have distinct stacking sequences. Typically, the 2H phase (Fig. 4b) follows an "AB" stacking sequence along the $\langle 001 \rangle_{2H}$ directions, while the 4H phase (Fig. 4c) is identified as a characteristic packing sequence of "ABCB" in the $\langle 001 \rangle_{4H}$ directions. Moreover, random or well-defined assembly of different phases in Au nanomaterials would result in heterophases, *e.g.*, 4H/fcc[32] and fcc-2H-fcc[59] (Fig. 4d and e). In this section, Au nanomaterials with different unconventional phases synthesized using the [Au(I)-oleylamine] complex through different routes are introduced, and the formation
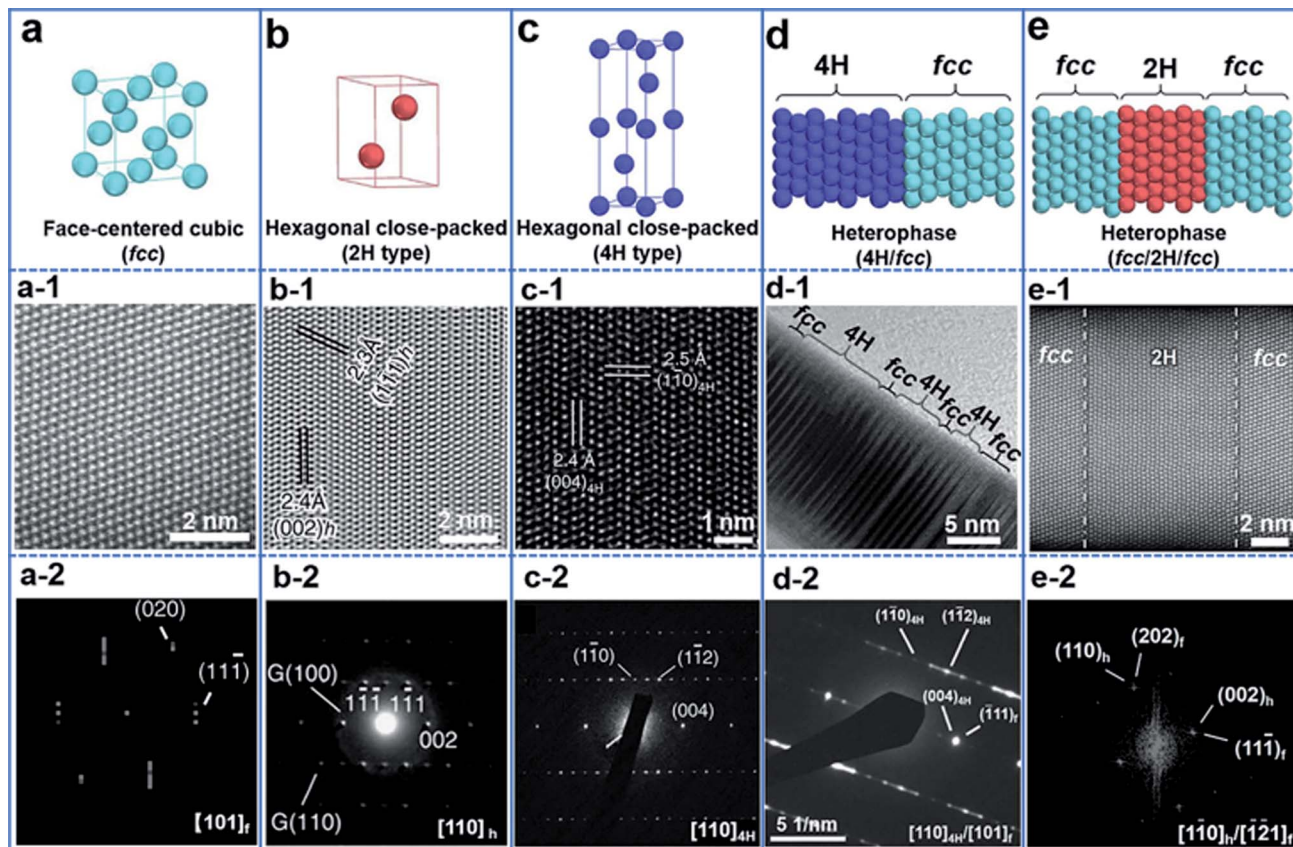
This journal is © The Royal Society of Chemistry 2021

J. Mater. Chem. A, 2021, **9**, 19534–19553 | **19541**

Fig. 4 Schematic atomic models of the different phases and heterophase structures of Au nanomaterials: (a) fcc, (b) 2H, (c) 4H, (d) 4H/fcc, (e) fcc-2H-fcc. Reproduced with permission.[31] Copyright 2020, American Chemical Society. (a-1, a-2) A representative high-angle annular dark-field scanning transmission electron microscopy (HAADF-STEM) image taken from the fcc region of a Au nanorod (NR) and the corresponding selected-area fast Fourier transform (FFT) pattern. Reproduced with permission.[59] Copyright 2020, Springer Nature. (b-1, b-2) HRTEM image taken from a small area of a typical Au square sheet (AuSS) oriented perpendicular to $[110]_h$ and the corresponding selected area electron diffraction (SAED) pattern of a AuSS on GO sheets. Reproduced with permission.[41] Copyright 2011, Springer Nature. (c-1, c-2) Aberration-corrected HRTEM images taken from the center of a Au nanoribbon (NRB) and the corresponding SAED pattern taken along the $[110]_{4H}$ zone axis. Reproduced with permission.[39] Copyright 2015, Springer Nature. (d-1, d-2) HRTEM image of a 4H/fcc Au NR displaying alternating 4H and fcc phases and the corresponding SAED pattern taken from the zone axes of $[110]_{4H}/[101]_f$. Reproduced with permission.[32] Copyright 2017, WILEY-VCH. (e-1, e-2) A representative HAADF-STEM image taken from a small region of an fcc-2H-fcc Au NR and the FFT pattern of an fcc-2H-fcc Au NR taken from the zone axes of $[110]_h/[121]_f$. Reproduced with permission.[59] Copyright 2020, Springer Nature.

mechanisms, classified as the size effect, stacking fault, oxidative etching, epitaxial growth and geometrical frustration effect, are summarized.

2.2.1 Size effect. Theoretical calculations suggested that there could be a compensation effect between the bulk energy of a nanomaterial and its overall surface energy. Under ambient conditions, the bulk energy of a metal nanomaterial with a conventional phase is lower than that of its unconventional counterpart, while the surface energy of a metal nanomaterial with a conventional phase is higher than that of its unconventional counterpart.[80,81] In the meantime, as the dimension of a nanomaterial reduces, its increasing surface-to-volume ratio makes its surface energy dominant in the total system energy.[82] As a result, there could exist a threshold size value, below which the lower surface energy of the unconventional phase determines its lower system energy, even if it possesses higher bulk energy than its conventional counterpart.[83] This is proposed as the size effect on the phase of nanomaterials.[84,85] Therefore, it

becomes possible to stabilize unconventional phase in Au nanomaterials through size control.

The synthesis of 2H AuSSs[41] and 2H/fcc Au nanosheets[42,56] demonstrates the size effect on the stabilization of the unconventional crystal phase in Au nanomaterials. In 2011, Huang *et al.* reported the synthesis of pure 2H AuSSs on graphene oxide (GO) templates by reducing $HAuCl_4$ with oleylamine in a mixture of hexane and ethanol for 16 h.[41] The as-synthesized 2H AuSSs possess an edge length of 200–500 nm and a thickness of 2.4 ± 0.7 nm and only contain around 16 Au atomic layers in the thickness direction. Typically, their square basal planes are perpendicular to the $[110]_h$ direction, following a stacking sequence of "AB" in the $[001]_h$ direction (Fig. 4b-1 and b-2), and the $(\bar{1}12)_h$ planes enclose the four sides. A time-dependent experiment was carried out to illustrate the formation mechanism (Fig. 5a) of the 2H AuSSs by characterizing the intermediate products. The [Au(ı)-oleylamine] complex first self assembled into a square-like supramolecular structures *via* the

19542 | *J. Mater. Chem. A*, 2021, **9**, 19534–19553

This journal is © The Royal Society of Chemistry 2021

aurophilic interaction,[86] which would form small Au seeds (step 1) and then gradually fuse into the fcc dendritic structures with a high crystal defect density (step 2). The oxidative etching and smoothing of the dendritic structure accompanying the phase evolution from fcc to 2H resulted in the formation of a thinner square-like center (step 3), which finally led to the formation of well-shaped 2H AuSSs on GO sheets. It is worth noting that the AuSSs grew thicker from 2.4 to 6 nm with the prolonged reaction time of 28 h, meanwhile the pure 2H phase became less stable and fcc segments appeared, resulting in the formation of alternating 2H/fcc domains. Therefore, Huang et al. proposed

that the pure 2H AuSSs were formed due to the size effect, and a thickness of <6 nm could help to stabilize the pure 2H phase in the AuSSs.

In addition, the 2H/fcc heterophase can also be synthesized by the secondary growth of Au on 2H AuSSs to form AuSPs.[56] The side length of the AuSPs is similar to that of 2H AuSSs, but the thickness showed a different distribution. The thin center (∼5 nm) of the AuSPs is typically in the 2H/fcc heterophase, while a pair of thicker opposite edges (∼7.3 nm) exhibit a defect-free fcc phase. The thickness-induced partial 2H-to-fcc phase transformation occurred during the formation from AuSSs to
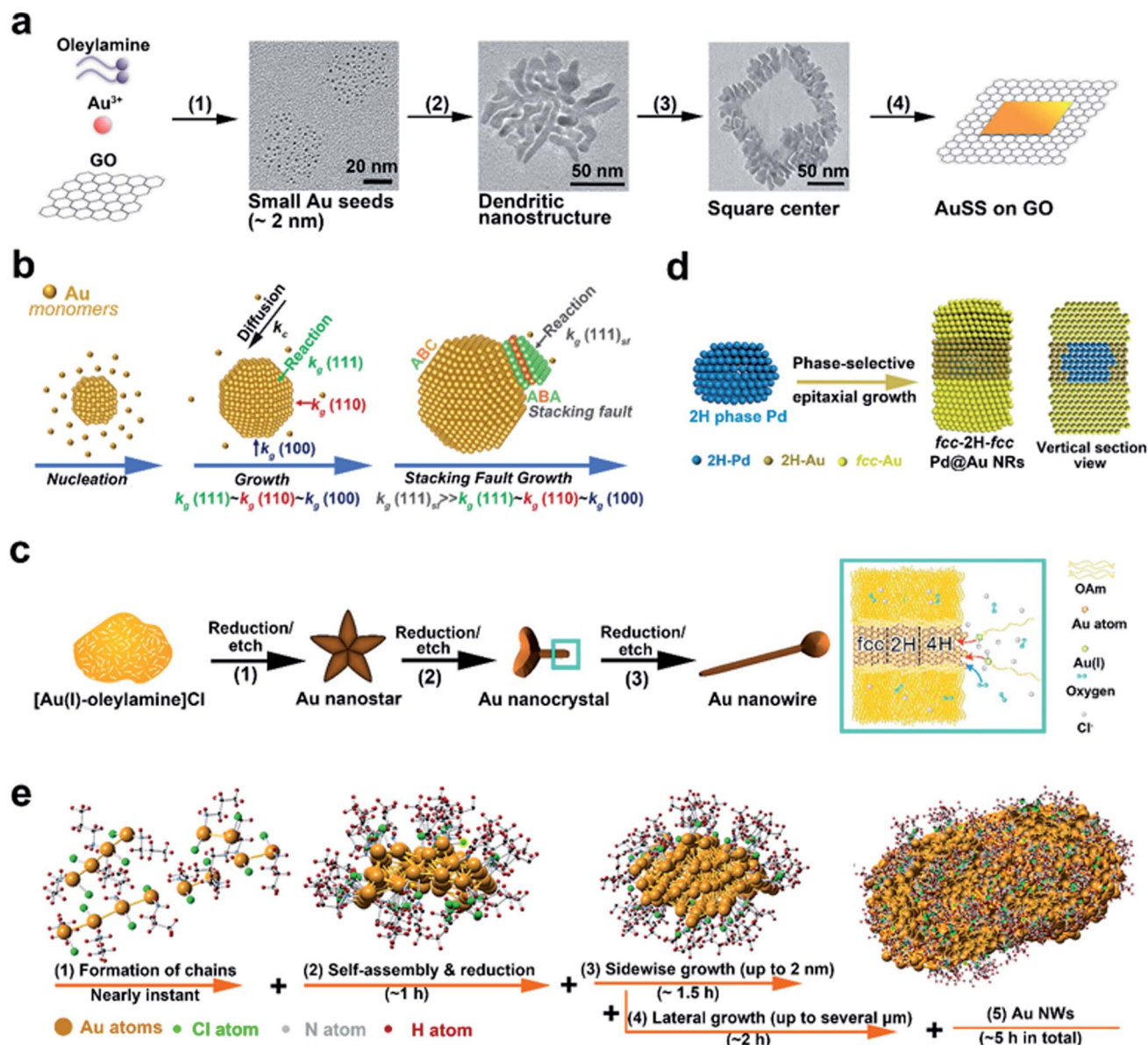

Fig. 5 (a) Scheme showing the formation and dimensional evolution process of 2H Au square sheets. Reproduced with permission.[41] Copyright 2011, Springer Nature. (b) Schematic illustration of the stacking fault growth mechanism of hcp/fcc Au NWs. Reproduced with permission.[94] Copyright 2020, The Royal Society of Chemistry. (c) Schematic illustration of the growth and morphology evolution process of hcp/fcc Au NWs under the oxidative etching effect. Reproduced with permission.[58] Copyright 2019, American Chemical Society. (d) Schematic illustration showing the formation process of fcc–2H–fcc Pd@Au NRs through epitaxial growth. Reproduced with permission.[60] Copyright 2020, American Chemical Society. (e) Schematic illustration of the formation of tetrahedrally close packed (tcp) Au NWs through the geometrical frustration effect. Reproduced with permission.[57] Copyright 2018, American Chemical Society.

AuSPs. At the center parts, fcc segments and stacking faults were formed due to the increasing thickness and the random distribution of the fcc phase. As for the edge parts, once the fcc phase appeared, they can grow both in lateral and vertical directions to form defect-free fcc structures. Very recently, Liu *et al.* reported the one-pot synthesis of free-standing 2H/fcc heterophase Au square-like nanosheets,[42] which have a similar structure to the AuSPs synthesized by Huang *et al.*[56] The as-synthesized nanosheets have an average edge length of 416 ± 160 nm and thickness of 8 nm. The formation of the 2H/fcc heterophase is therefore likely a result of the size effect, since Huang *et al.* proposed that the pure 2H phase could not be stabilized in Au nanosheets with a thickness larger than 6 nm.[41]

The size effect on the phases of Au nanomaterials was also observed in 1D Au nanostructures with different diameters or widths. In another work, Huang *et al.* synthesized ultrathin Au NWs with an unconventional phase on GO templates by heating HAuCl$_4$ and oleylamine solution at 55 °C for 36 h.[43] The as-synthesized Au NWs have an average diameter of 1.6 nm and contain 2H domains. The time-dependent experiment revealed that Au seeds of 2 nm were first formed from the [Au(ɪ)-oleylamine] complex and grew into short rod-like structures, which would then assemble into discontinuous chains and age to form the ultrathin Au NWs. In comparison, if the reaction solution was heated for 10 h and then aged under ambient conditions for 2 days, tadpole-shaped Au NWs with an enlarged head were obtained. A similar size-induced phase transformation was observed, *i.e.*, the thicker head segments (∼12–16 nm) exhibited a defect-free fcc phase, while the tail regions (∼7 nm) contained the 2H/fcc heterophase. Therefore, the formation of mixed 2H and fcc structures in 1D Au NWs was related to the diameter variation, another evidence of the size effect. Compared with the synthesis of 2H AuSSs, solvent polarity might play a role in influencing the morphology and crystal phase of Au nanomaterials, *i.e.*, pure hexane for 2H/fcc NWs[43] and the mixture of hexane and ethanol for AuSSs.[41]

In addition to the unconventional 2H phase, the size effect can also explain the formation of the conventional 4H phase. Theoretical calculations suggested that the cohesive energy difference (per atom of Au nanomaterials) between 4H and fcc phases is lower than the difference between 2H and fcc phases.[79] Hence, it is theoretically possible to synthesize 4H Au nanomaterials. In 2015, Fan *et al.* reported the stabilization of colloidal 4H Au NRBs by reducing the HAuCl$_4$ precursor in a mixture of oleylamine and hexane under the assistance of 1,2-dichloropropane (1,2-DCP).[39] The as-synthesized 4H Au NRBs grew along the $[001]_{4H}$ direction (Fig. 4c-1 and c-2), showing a length of 0.5–6.0 μm, width of 15.0–61.0 nm and thickness of 2.0–6.0 nm. The initially formed ultrathin Au NWs with a diameter of 1.4–2.0 nm contained 2H segments and many random stacking faults, which then evolved into ribbon-like structures, accompanying a 2H to 4H phase transformation. The phase transformation from the 1D 2H-containing Au NWs to 1.5D (or quasi-2D) 4H Au NRBs was believed to drive by the energy difference.[78]

Besides the pure 4H NRBs, the narrow energy difference between 4H and fcc phases may also contribute to the formation of 4H/fcc heterophase Au NRs.[78,87] In 2017, Chen *et al.* reported the high-yield and one-pot synthesis of alternating 4H/fcc heterostructured Au NRs by reducing the HAuCl$_4$ with oleylamine at 70 °C.[32] The as-synthesized Au NRs show diameters of ∼11–27 nm and lengths of ∼200–1000 nm with randomly distributed 4H and fcc segments (Fig. 4d-1 and d-2).[32] Time-dependent experiments suggested that the fcc ultrathin Au NWs (∼3 nm) were formed initially, which then reconstructed to form wider and shorter NRs.[87] The 4H phase started to appear during the widening of NWs. Different from the reaction conditions of pure 4H Au NRBs,[39] the absence of 1,2-DCP and the higher temperature might cause faster formation of the 4H phase, leading to the competitive growth between 4H and fcc phases during the diameter evolution and the coexistence of 4H and fcc phases in individual Au NRs.

In brief summary, size control is a critical strategy in controlling the phase of Au nanomaterials. It can be realized by modifying the reaction conditions based on the [Au(ɪ)-oleylamine] system, *i.e.*, adjusting the reaction temperature, using a template and/or adding suitable chemicals, leading to the formation of Au nanomaterials with unconventional phases.

2.2.2 Stacking fault. The formation of stacking faults during the growth of nanocrystals is another feasible explanation of the formation of unconventional phases, particularly heterophases with alternating stacking sequences of their close-packed planes in 1D nanomaterials. Stacking fault is a kind of short-range crystallographic planar defect along the regular stacking sequence, which results from the insertion or missing of crystallographic planes.[88,89] The generation of stacking faults in metals depends on their stacking fault energy. It is much easier to generate stacking faults in some noble metal nanomaterials, *e.g.*, Au and Ag, since they lie in a low stacking fault energy regime along their closed packed direction.[70,79,90] Three basic stacking faults have been observed, including twin stacking fault, intrinsic stacking fault (a layer missed) and extrinsic stacking fault (an extra plane inserted).[91–93] Importantly, when orderly connected, these stacking faults could lead to the formation of unconventional phases. For example, the formation of 2H or 4H phase segments in Ag nanoplates has been observed to be the continuous connection of more than two intrinsic or extrinsic stacking faults, respectively.[91] Moreover, the presence of stacking faults could induce extra atomic steps or kinks on the surface and affect the surface energy of Au nanomaterials.[88,93] Therefore, the occurrence of stacking faults and the induced surface energy change may contribute to the formation and stabilization of short-range unconventional phases, resulting in a heterophase in Au nanomaterials.

In 2010, Kura *et al.* synthesized Au NWs with mixed fcc and hcp phases by reducing HAuCl$_4$ in oleylamine.[55] They proposed that the Au NWs were generated by the restructuring of nanoparticles or agglomerates formed from the R-NH$_2$ClAu$^+$ intermediates. The HRTEM image taken from the ⟨110⟩ direction showed that the atomic stacking sequence changed from "ABCA" to "ACBC" and "ABAB" in some segments. The occurrence of intrinsic and extrinsic stacking faults during the Au NW growth process may cause the formation of hcp segments in the Au NWs. As for the alternating 4H/fcc heterostructured Au

19544 | *J. Mater. Chem. A*, 2021, **9**, 19534–19553

This journal is © The Royal Society of Chemistry 2021

NRs introduced in Section 2.2.1, the stacking fault mechanism might be another reasonable explanation for the formation of the 4H phase, *i.e.*, the appearance of continuous extrinsic stacking faults.[32]

In 2020, Moraes *et al.* obtained the tadpole-like Au NWs with a mixture of hcp and fcc phases.[94] Different from Huang *et al.*'s work,[43] the tadpole-like Au NWs were synthesized without the assistance of GO sheets. The larger spherical heads show a defect-free fcc Au structure, while the diameter of the tail regions gradually decreases, showing a random distribution of fcc and hcp phases. The authors proposed that the heterophase in the tail region was formed due to the stacking fault mechanism, and three factors, including low temperature, moderate stirring, and oleylamine as the surfactant, could lead to the formation of stacking faults in the tail regions. Firstly, the low temperature could assist the stabilization of stacking faults. Secondly, oleylamine is critical to the generation of stacking faults. It was reported that the rearrangement of the oleylamine shell could contribute to the formation of twin stacking faults.[71] Thirdly, the low stirring rate would alter the diffusion-controlled growth mechanism into the stacking fault growth mechanism after the formation of the fcc head (Fig. 5b). The decreased local concentration of the Au precursor resulted in the growth of random stacking faults on the (111) facet to form the tail part. In the stacking fault growth step (Fig. 5b), the growth rate of the stacking fault (111) facet $[k_g(111)_{sf}]$ would be much higher than that of other facets $[k_g(hkl)]$. As a result, the tadpole-like Au NWs with 60% hcp phase and 40% fcc phase were obtained.

Thus, the low stacking fault energy of Au could make the occurrence of stacking faults more energetically preferential under the mild synthesis condition. The formation of unconventional phase segments could be regarded as the appearance of continuous stacking faults in 1D Au nanostructures, which often lead to the formation of heterophases.

2.2.3 Oxidative etching. Since the initial study of the role of oxidative etching in single-crystalline Ag nanoparticle synthesis by Xia's group in 2004,[76] it has been widely used to re-shape metal nanocrystals through atomic addition and subtraction to control the nucleation and growth process.[52,95,96] Normally, oxidative etching selectively takes place in surface defect sites (*i.e.*, twin defects), as these sites have a higher energy than the single-crystal zones and thus are more sensitive to an oxidative environment.[97,98] Meanwhile, the oxidative etching effect can also compete with the reduction reaction of the metal precursors,[97] *i.e.*, the pre-formed zero-valent atoms can be oxidized into their ionic states due to the existence of oxidative species (*e.g.*, oxygen or Fe(III)/Fe(II)), ligands and/or corrosive anions (such as Cl⁻).[52,99] When the strength of the oxidative etching effect is strong enough, the nucleation and growth mechanism of metal nanocrystals will be altered from a thermodynamically controlled pathway into a kinetically controlled pathway.[100] Therefore, controlling the reduction kinetics *via* oxidative etching is a feasible approach to obtain metal nanomaterials with unconventional phases.[88] For instance, Ag nanodisks with a random hcp phase and stacking faults instead of its thermodynamically stable fcc phase could be synthesized when the

reduction rate became adequately slow under the effect of the strong etching.[98,101] As for the synthesis of Au nanocrystals, the oxidative etching effect is commonly caused by the O_2/Cl⁻ pair and/or ligands (*e.g.*, amine), which are powerful etching species for both the formed nuclei and seeds.[66,102–104] They could be used to induce the kinetically controlled formation of metastable nanostructures of Au *via* oxidative etching.

Wang *et al.* proposed an oxidative etching assisted route to synthesize Au NWs with randomly distributed hcp/fcc heterophases in the mixture of $HAuCl_4$, $CuCl_2$ and oleylamine at 160 °C for 4 min.[58] Apart from 2H and 4H phases, some segments containing 6H and 8H phases, with "ABCACB" and "ABCBCBAB" stacking sequences along the $[001]_h$ direction, respectively, were also observed in the NWs. In this reaction, the O_2/Cl⁻ pairs and oleylamine acted as etchants and reducing agent, separately, and the growth of Au nanocrystals was dominated by kinetic control. The initially formed mesoporous [Au(I)-oleylamine] complexes would evolve to form the penta-twinned fcc Au nanostars assisted by Cu^{2+} (Fig. 5c, step 1), which could be etched owing to their large lattice distortion.[104] During etching and the fast reduction, the Au nanostar transformed into a Au nanocrystal (Fig. 5c, step 2) and further grew into a NW (Fig. 5c, step 3). Control experiments confirmed the etching effect of O_2/Cl⁻ pairs, and the absence of O_2 or Cl⁻ only led to the formation of fcc Au nanostars or NPs.

In addition, well-defined fcc-2H-fcc heterophase Au NRs by reducing the mixture of $KAuCl_4$, oleylamine and *n*-dodecyl-amine were synthesized by Fan *et al.*[59] The two fcc segments were located at each end of the NRs along the $[111]_f$ direction (Fig. 4e-1 and e-2), whereas the 2H segment was situated in the middle of the NRs along $[001]_h$ direction, resulting in the formation of a sandwich-like structure. Notably, it was found that O_2 played a significant role in the formation of these NRs, and the NRs could only be synthesized by purging O_2 into the reaction solution. It can be speculated that the oxidative etching effect may contribute to the formation of such a unique heterophase Au nanostructure. The Cl⁻ ions released from the Au precursors could pair with the O_2, leading to a more effective oxidative etching process.[104] The enhanced oxidative etching effect might alter the reduction reaction into kinetic control,[100] resulting in the formation of the metastable fcc-2H-fcc heterophase Au NRs.

To briefly summarize, a sufficient amount of Cl⁻/O_2 pairs in the [Au(I)-oleylamine] system could force the nucleation and growth of Au nanomaterials to fall into kinetic control rather than thermodynamic control, facilitating the formation and stabilization of the unconventional phase.

2.2.4 Epitaxial growth. Epitaxial growth, the oriented deposition of guest crystalline materials on the surface of a host crystalline substrate,[105] is another important strategy to obtain unconventional phases in nanomaterials. Specifically, when the host metal nanomaterials have unconventional phases or their conventional phase is different from the conventional phase of the guest materials, it is possible to obtain guest nanomaterials with unconventional phases *via* epitaxial growth. Normally, a relatively small lattice mismatch (usually <5%) between two metals is demanded to realize such crystal phase based epitaxial

This journal is © The Royal Society of Chemistry 2021

J. Mater. Chem. A, 2021, **9**, 19534–19553 | **19545**

growth, since the interfacial energy difference of the hybrid nanostructures can be minimized.[106,107] The crystal phase based epitaxial growth has several advantages compared with direct bottom-up synthesis methods. Heterogeneous nucleation during the epitaxial growth process endows this step with a lower energy barrier than homogeneous nucleation,[108] and therefore it is feasible to manipulate the growth pattern.[109] Additionally, when the host nanomaterials possess a certain specific crystal phase and morphology, the guest metal could synchronously duplicate both their phase and morphology.[109–111] For instance, fcc ruthenium (Ru) icosahedral nanocages could be obtained by replicating the surface atomic arrangement of the fcc palladium (Pd) nanocrystals *via* epitaxial growth.[112] Hence, it is rational to deposit Au atoms on other nanomaterials to prepare novel metastable nanostructures.

Different from Fan's work,[59] the well-defined fcc-2H-fcc heterophase Au short NRs can also be synthesized *via* epitaxial growth. In 2020, Ge *et al.* reported the synthesis of fcc-2H-fcc heterophase Pd@Au NRs through a facet-directed crystal-phase-selective epitaxial growth of Au on 2H Pd NPs (Fig. 5d).[60] The author proposed that the formation of the unique Pd@Au nanostructure might arise from the selective deposition of Au atoms on distinct exposed facets of 2H Pd NPs. Since the $(002)_h$ plane of 2H Pd and $(111)_f$ plane of fcc Au possessed identical 6-fold symmetry and similar lattice constants ($d = 2.81$ and 2.88 Å, respectively), fcc Au could deposit on the $(002)_h$ planes of 2H Pd to form the two fcc ends in the fcc-2H-fcc NRs.[113,114] Meanwhile, on other exposed facets of Pd seeds, 2H Au was epitaxially grown to form the middle part of the NRs.

Therefore, by choosing nanocrystals possessing similar lattice parameters to Au as seeds, nanocrystal@Au hybrid nanostructures can be obtained through epitaxial growth. It could be an effective and relatively simple method to expand the library of the crystal phase of Au nanomaterials.

2.2.5 Geometrical frustration effect. The geometrical frustration effect was proposed by Vargas *et al.* to understand the formation mechanism of the tcp structure observed in Au NWs (Fig. 5e).[57] During the synthesis, when the molar ratios of oleylamine/Au and TIPS/oleylamine were ~10–20 and ~2–3, respectively, short chain-like $[Cl-Au^I-NH_2-R]_n$ complexes were first formed due to the interchain aurophilic interactions (Fig. 5e, step 1), which self-assembled and aggregated owing to the excluded volume effect (Fig. 5e, step 2).[115] Subsequently, the reduced Au(0) grew into clusters with diameters of up to 2 nm (Fig. 5e, step 3), which continued to elongate in the lateral direction (Fig. 5e, step 4) to gradually evolve into 1D NWs in lengths of micro meters (Fig. 5e, step 5). The authors attributed the formation of the unusual tcp structure, which can be considered as an incorporation of distorted icosahedra and larger size polyhedra, to the geometrical frustration effects. Specifically, the assembly of Au atoms had the tendencies to keep high packing density while maintaining low atomic-level tensile stress, which ultimately resulted in the formation of the ultrathin, cylindrical NWs with a tcp structure.

3. Applications

Owing to their outstanding physicochemical properties, Au nanomaterials have attracted considerable attention in various applications. In the following sections, the utilization of Au nanomaterials synthesized from the [Au(I)-oleylamine] system in two most widely studied applications, including catalysis and electronic devices, are chosen for detailed discussion.

3.1 Catalysis

Because of the intriguing electronic structures and chemical stability, Au nanomaterials exhibit outstanding performances in various catalytic reactions. In this section, we summarize the catalytic applications of Au nanomaterials synthesized from the [Au(I)-oleylamine] system in the carbon dioxide reduction reaction (CO_2RR), the oxygen reduction reaction (ORR), the nitrogen reduction reaction (NRR), CO oxidation, and the photocatalytic reaction.

3.1.1 Carbon dioxide reduction. The CO_2RR has attracted increasing attention as it is a promising approach to convert the greenhouse gas CO_2 into useful chemicals and fuels such as CO, formic acid, ethylene and alcohols.[116–119] Au exhibits the highest activity and selectivity in reducing CO_2 to CO among polycrystalline metals.[120] Studies suggested that the performance of CO_2 reduction of Au nanomaterials can be further enhanced by modulating their size, shape and crystal phase.[31,121]

In 2013, Zhu *et al.* investigated the size-dependent catalytic activity of Au NPs for CO_2 electroreduction.[122] When the size of Au NPs increased from 4 nm to 10 nm, the activity of the Au NPs showed a nonmonotonic trend and 8 nm Au NPs exhibited a maximum Faradaic efficiency (CO) (FE(CO)) of up to 90% at −0.67 V *versus* (*vs.*) the reversible hydrogen electrode (RHE) (Fig. 6a). In addition, DFT computations suggested that edge sites on the Au NPs are active for CO formation while corner sites favor H_2 evolution. The edge active sites showed lower energy barriers toward the formation of the *COOH intermediate, which is the critical step for the activation of CO_2. This investigation suggested that an optimal ratio between the edge and corner sites could be important to the high catalytic activity of Au NPs. In addition to Au NPs, Au nanomaterials with other morphologies could also be useful in maximizing the distribution of the active sites. For example, another work by Zhu *et al.* showed that Au nanomaterials with 1D geometry could exhibit high abundance of edge sites.[123] Due to a high density of CO_2 active sites exposed on the surface, ultrathin Au NWs with ~2 nm width exhibited a significant enhancement of CO_2 reduction activity. The FE(CO) reached 94% at a low potential of −0.35 V *vs.* RHE. DFT calculations suggested that Au NWs with abundant edge sites can stabilize the *COOH and weaken the *CO binding, which facilitates the activation of CO_2 to *COOH and the release of CO from active sites, respectively.

Besides tuning the size and morphology of Au nanomaterials, crystal phase control has emerged as an effective strategy to boost the CO_2RR performance of Au nanocrystals.[59,111] Recently, Wang *et al.* investigated the crystal phase-dependent CO_2RR activity of Au nanomaterials, including 4H

19546 | *J. Mater. Chem. A*, 2021, **9**, 19534–19553
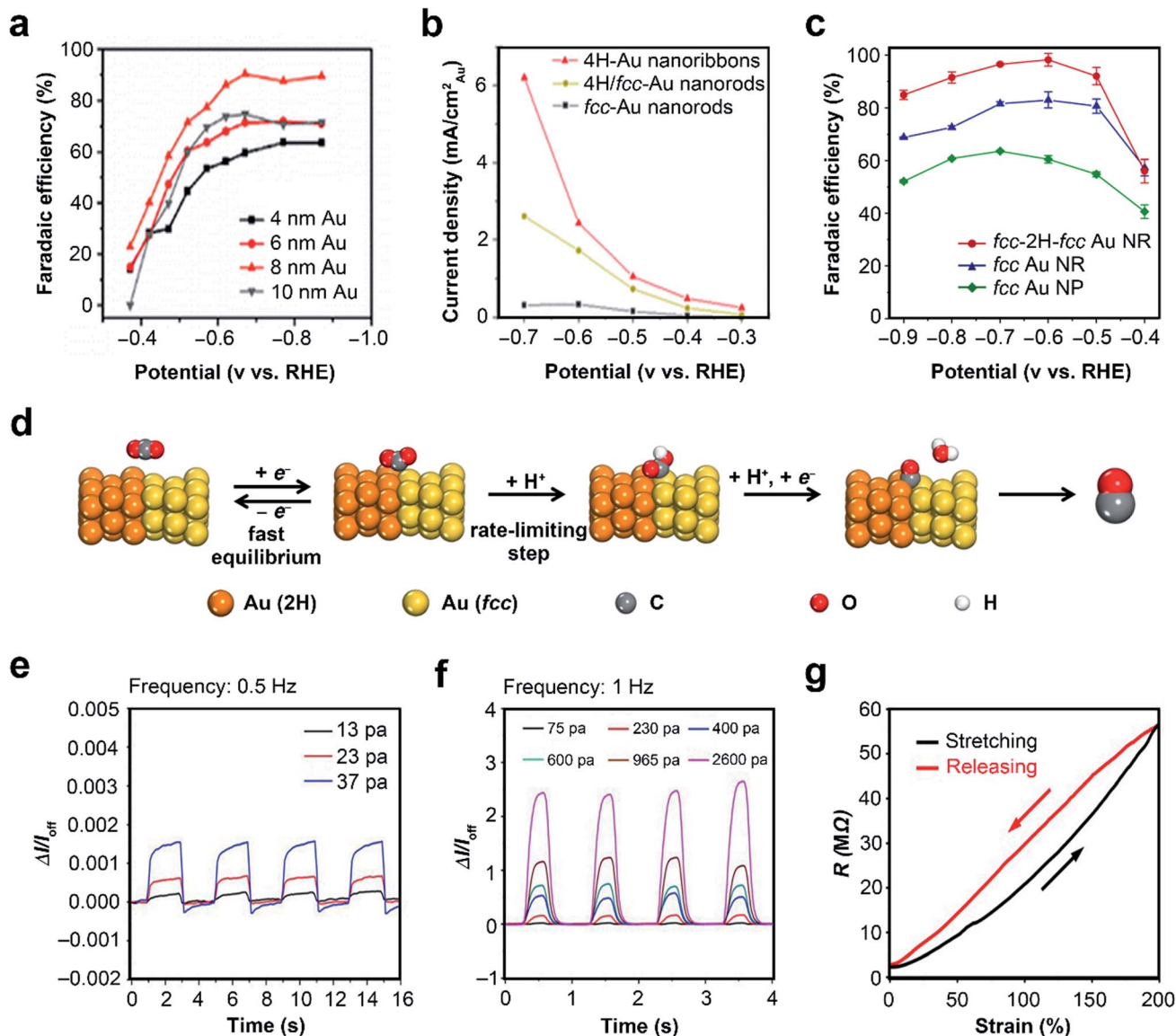
This journal is © The Royal Society of Chemistry 2021

Fig. 6 Application of Au nanomaterials synthesized using the [Au(I)-oleylamine] complex. (a) The carbon monoxide (CO) faradaic efficiency of Au NPs with different sizes at potentials from −1.0 to −0.4 V *versus* (*vs.*) the reversible hydrogen electrode (RHE). Reproduced with permission.[122] Copyright 2013, American Chemical Society. (b) The CO current density of the three types of Au nanocrystals at potentials from −0.7 to −0.3 V *vs.* RHE. Reproduced with permission.[124] Copyright 2020, American Chemical Society. (c) The CO faradaic efficiency of various Au nanostructures at potentials from −0.9 to −0.4 V *vs.* RHE. Reproduced with permission.[59] Copyright 2020, Springer Nature. (d) Scheme of carbon dioxide reduction pathway on the surface of heterophase fcc-2H-fcc Au NRs. Reproduced with permission.[59] Copyright 2020, Springer Nature. (e) Plot of the current response of the sensor as a function of time (pressure input frequency: 0.5 Hz) for various applied pressures. (f) Plot of the current response of the sensors against time (pressure input frequency: 1 Hz) for the applied pressures in the range from 75 Pa to 2600 Pa. Reproduced with permission.[146] Copyright 2014, Springer Nature. (g) Plot of electrical resistance changes of the strain sensor against strain changes of 0−200−0% with the stage moving speed at 3 mm s⁻¹. Reproduced with permission.[147] Copyright 2015, WILEY-VCH.

Au NRBs, 4H/fcc Au NRs and fcc Au NRs (Fig. 6b).[124] They found that the selectivity and activity of Au nanocatalysts for CO production exhibited a trend of 4H Au NRBs > 4H/fcc Au NRs > fcc Au NRs, suggesting that Au nanomaterials with the 4H phase possess highly active sites for converting CO_2 into CO. Importantly, the result of underpotential deposition of lead indicated that 4H Au NRBs exhibit a much higher fraction of undercoordinated sites compared with 4H/fcc Au NRs and fcc Au NRs. Further DFT calculations revealed that the undercoordinated sites on the surface of 4H Au are more active than the (111)

surfaces of fcc Au. Experimental and theoretical studies indicated that the enhancement of the CO_2RR performance of 4H Au NRBs can be attributed to the presence of a high density of undercoordinated sites on the surface of 4H Au NRBs. In another work, heterophase fcc-2H-fcc Au NRs were used as an electrocatalyst for the reduction of CO_2 to CO.[59] Compared with the common fcc Au NPs and fcc Au NRs, the fcc-2H-fcc Au NRs showed a lower onset potential, much higher FE and current density towards the CO formation. Specifically, the fcc-2H-fcc Au NRs showed the highest FE(CO) of 98.2% at −0.6 V *vs.*

This journal is © The Royal Society of Chemistry 2021

J. Mater. Chem. A, 2021, **9**, 19534–19553 | **19547**

RHE, much higher than that of the FE(CO) on fcc Au NRs (81.6%) and fcc Au NPs (63.6%) (Fig. 6c). Importantly, the fcc-2H-fcc Au NRs exhibited a much smaller Tafel slope of 64.9 mV dec^{-1}, indicating a faster electron exchange rate on fcc-2H-fcc Au NRs than on the fcc Au NRs and NPs. Free energy calculations for the CO_2RR pathways suggested that the 2H surface and 2H/fcc interface possess low energy barriers to form *COOH, which is the rate-limiting step for the formation of CO (Fig. 6d). The enhanced CO_2RR catalytic performance observed from the heterophase fcc-2H-fcc Au NRs can be ascribed to the presence of the unconventional 2H phase and 2H/fcc interface, which provide energetically favorable pathways for the formation of the reaction intermediates. Very recently, the epitaxially grown fcc-2H-fcc heterophase Pd@Au core–shell NRs also demonstrated excellent performance towards electrochemical CO_2RR.[60] Specifically, the FE(CO)s on fcc-2H-fcc Pd@Au NRs were above 90% in a wide potential window, better than the FE(CO)s on fcc-Au NRs, fcc Pd@Au NPs, and 2H-Pd NPs. The authors proposed that the synergistic effect of internal strain in the Au shell and the presence of 2H phase and 2H/fcc phase boundaries contribute to the enhanced CO_2RR performance.

In addition, Gao *et al.* found that the Au surface absorbed by oleylamine can suppress the hydrogen evolution reaction and enhance the performance of the CO_2RR.[125] For as-synthesized Au nanoparticles capped with oleylamine, the FE(CO) remained >93% in a wide potential range of −0.4 to −0.8 V *vs.* RHE. In contrast, after removal of the absorbed oleylamine on the Au NPs by annealing in air, the obtained sample exhibited low activity towards the CO_2RR. Interestingly, the re-wrapping of oleylamine can restore most of the catalytic activity and selectivity for the CO formation. The authors proposed that oleylamine is likely to absorb on the low-coordinated sites, which are active for the hydrogen evolution reaction, to minimize the surface energy. The occupation of hydrogen evolution sites allows more electrons and H$^+$ to participate in the CO evolution, which may lead to the enhanced CO_2RR performance.

3.1.2 Oxygen reduction reaction. Due to the sluggish kinetics of the multielectron transfer reaction, the ORR remains a bottleneck of the development of proton-exchange membrane fuel cells.[126,127] In 2010, Lee *et al.* synthesized monodisperse polycrystalline Au NPs in the sizes of 3 nm, 6 nm, and 8 nm to explore their ORR catalytic activity.[128] The 3 nm Au NPs synthesized at room temperature or above exhibited a better onset potential than the 6 nm Au NPs because the higher surface-to-volume ratio of 3 nm NPs provides more abundant surface atoms for oxygen binding. Interestingly, the 8 nm Au NPs prepared at a low temperature of 3 °C exhibit a even more positive onset potential than the 3 nm Au NPs. The authors proposed that the twinned boundaries formed at the lower reaction temperature could provide more defects on the surface of the catalyst and may offer more active sites for the ORR. In addition to the degree of disorder in the polycrystalline structure, the authors believed that the ease of oleylamine removal on the polycrystalline Au NPs could also contribute to the enhanced ORR activity.

3.1.3 Nitrogen reduction reaction. Electrochemical NRR is considered a green and environmentally friendly approach for the production of ammonia.[129,130] Recently, Chen *et al.* synthesized monodisperse Au NPs with sizes tunable from 4 nm to 10 nm and investigated their size-dependent NRR activity.[131] They found that 8 nm Au NPs exhibit the highest NRR activity toward ammonia formation with a faradaic efficiency and formation rate of 5.79% and 17.49 μg h^{-1} mg$_{Au}^{-1}$, respectively. DFT calculations suggested that 8 nm Au NP possesses the optimal proportion of edge and corner sites, which contribute to the enhancement of NRR activity.

3.1.4 Carbon monoxide oxidation. CO oxidation is a useful approach to mitigate environmental and health problems caused by CO in the atmosphere.[132,133] Because of the outstanding catalytic activity of Au nanomaterials in the CO oxidation reaction at low temperature, they have attracted considerable attention. For instance, Peng *et al.* synthesized monodispersed polycrystalline Au NPs with icosahedral shapes and various sizes ranging from 1 nm to 10 nm.[134] They found that 6 nm NPs deposited on a porous carbon support exhibited 100% CO oxidation conversion at a low temperature of −45 °C. The authors proposed that the presence of the twinned boundaries in the polycrystalline Au NPs contributes to their enhanced catalytic performance.

3.1.5 Photocatalytic reaction. Photocatalysis is a sustainable and green technology that converts solar energy into useful fuels and chemicals.[135] Au nanomaterials exhibit outstanding photocatalytic activity in various reactions due to their strong localized surface plasmon resonance properties.[136] For example, Long *et al.* reported a Au-plasmon enhanced solar-to-hydrogen conversion on anatase TiO_2 nanosheets, and the conversion rate of solar-to-hydrogen conversion was improved 64 times.[137] They demonstrated that Au NPs can not only absorb and convert visible photons to free energetic electrons, but can also enhance the photocatalytic solar-to-hydrogen conversion activity *via* improving the formation rate of electron–hole pairs. Recently, the phase-dependent photocatalytic performance of Au nanomaterials was reported by Huang *et al.*[138] By using *in situ* surface-enhanced Raman spectroscopy, the hot-electron-induced photocatalytic *para*-nitrothiophenol reduction to *p,p′*-dimercaptoazobenzene on 4H and fcc Au nanomaterials was studied. Importantly, 4H Au NRBs showed the highest photocatalytic performance, which was about 8 and 6 times higher than that of fcc Au NWs and fcc Au NRs, respectively.

3.2 Electronic devices

Because of their excellent electrical conductivity, biocompatibility, and chemical inertness, Au nanomaterials have been regarded as promising active components in electronic devices, such as conductors and sensors.[139] In 2008, Wang *et al.* reported that a single-crystalline ultrathin Au NW as an electron conductor exhibited good electron conductivity.[49] Specifically, the resistivity and breakdown current density were measured to be 260 Ω nm and 3.5 × 10^{12} A m^{-2}, respectively, indicating it is a promising interconnect for nanoelectronic devices. It is worth noting that Au NWs are mechanically flexible and intrinsically

19548 | *J. Mater. Chem. A*, 2021, **9**, 19534–19553

This journal is © The Royal Society of Chemistry 2021

stretchable, which endow them with great potential as flexible and stretchable electrodes.[139,140] For example, Chen *et al.* developed a simple yet efficient method to fabricate stretchable and transparent superlattice nanomembranes with a thickness of 2.5 nm using Au NWs.[141] The ultrathin nanomembranes are mechanically flexible, optically transparent and electrically conductive, making them promising in applications in foldable electronic devices. However, the lack of connections between self-assembled Au NWs resulted in a high electrical resistance of 1142 kΩ sq^{-1}. Subsequently, the same group used a bottom-up self-assembly strategy to fabricate a mesh-like Au NW electrode.[142] The sheet resistance of this mesh-like thin film decreased by about 40 times compared with that of a non-meshed thin film they previously reported.[141] Importantly, the mesh-like electrode is easily transferrable, electrically stable, mechanically flexible and highly transparent, showing great potential in flexible optoelectronic devices. In addition, Maurer *et al.* demonstrated that Au NWs are suitable components for nanoimprinting inks due to their mechanical flexibility and self-assembly behavior.[140] By using direct nanoimprinting of self-assembled Au NWs, they fabricated flexible grid electrodes with high conductivities and transparencies, which are suitable for application in transparent flexible electronics. Recently, Au NWs have been developed to serve as stretchable electrodes of flexible fuel cells.[143,144] Compared with traditional fuel cells using rigid electrodes, stretchable fuel cells based on Au NW electrodes can be integrated into wearable and implantable electronics.

In addition to conductors, Au NWs have also been applied in sensors due to their outstanding sensitivity. In 2014, Kundu *et al.* developed a method to directly grow ultrathin Au NWs on various substrates, including graphene, borosil glass, Kapton, and oxide supports.[145] They demonstrated that direct growth of Au NWs on a flexible substrate (Kapton) can be used for strain sensing, chemical sensing, and biomolecule sensing. In another work, Gong *et al.* developed a low-cost, efficient, bottom-up method to fabricate a wearable and highly sensitive pressure sensor using Au UNWs.[146] Dynamic forces in a wide pressure range of 13 to 50 000 Pa could be detected by using this Au NW-based sensor (Fig. 6e and f). Importantly, this pressure sensor can operate at a battery voltage of 1.5 V and exhibit the merits of high sensitivity (>1.14 kPa^{-1}), a fast response time (<17 ms), and high stability (>50 000 cycles). Then, they used a drop-casting approach to fabricate micro meter-thin stretchable and sensitive wearable strain sensors using Au NWs.[147] This strain sensor can detect dynamic tensile strain in a wide range of 0.01–200% (Fig. 6g). In a follow-up work, after doping polyaniline microparticles into Au NW films, the sensitivity and conductivity of the film can be further increased by about ∼8 times and 10 times, respectively.[148] Importantly, after latex encapsulation, their sensors are fully water-resistant and exhibit excellent long-term durability.

4. Conclusion and perspective

In this review, we summarized the recent development of colloidal synthesis of Au nanomaterials with a controlled morphology and crystal phase using the [Au(ı)-oleylamine] complex. Oleylamine as the surfactant, reducing agent, and solvent plays an important role in tuning the size, shape, dimension and atomic packing sequence of the obtained Au nanocrystals. The possible growth mechanisms of Au nanomaterials with different morphologies and phases synthesized *via* the [Au(ı)-oleylamine] complex were discussed. The promising applications of oleylamine-capped Au were also highlighted.

Despite the considerable progress made so far, there are still some challenges in this research direction. First, the kinds of reported morphologies and phases of Au nanomaterials obtained *via* the [Au(ı)-oleylamine] complex need to be further extended. Second, although several growth mechanisms have been proposed to understand the formation of the unconventional Au phases, there is still a lack of *in situ* structure characterization to support these theories. Lastly, compared with fcc Au nanomaterials, the applications of Au nanomaterials with a metastable phase or heterophase are still finite, and more intriguing properties and potential applications of unconventional Au phases should be further discovered.

Despite the aforementioned challenges, there are also many opportunities to be explored in the study of the [Au(ı)-oleylamine] system. First of all, since oleylamine exhibits unusual behavior in the synthesis of Au nanomaterials with unconventional phases, it is highly desired to further synthesize other novel crystal phases of Au nanomaterials based on the [Au(ı)-oleylamine] system, which may be achieved by tuning the synthetic conditions, such as the solvent, temperature, pressure, surfactant, and additive. Besides the synthesis of other novel phases, it is of great importance to simultaneously control the phase and other structural characteristics, like the morphology, size, and dimensionality, of Au nanomaterials. This enables us to study the crystal phase-dependent properties of Au nanomaterials while the effect of other structural parameters can be neglected. Second, it is possible to obtain Au nanomaterials with novel structures by combining or transferring the [Au(ı)-oleylamine] system to other systems. For example, bent 4H Au NRBs could be obtained by transferring as-synthesized 4H Au NRBs *via* the [Au(ı)-oleylamine] system into a reaction mixture of *N,N*-dimethylformamide, polyvinylpyrrolidone and chloroform, which could be used as templates for the growth of the unusual 4H twinned nanokite.[149] Third, instead of wet-chemical synthesis, other synthetic approaches, such as electrochemistry and photochemistry, can be explored. The development of new synthetic strategies can facilitate low-cost and large-scale synthesis of Au nanomaterials and may also promote the formation of Au nanomaterials with a novel morphology or phase. Fourth, towards the practical applications, the rational design and synthesis of the M@Au (M represents earth-abundant early transition metals) heterostructure are of great significance, which can mitigate the problem of limited reserves and high cost of Au. Importantly, this kind of combination of Au with other metals can also tune the properties of Au, which could enhance the performance of Au nanomaterials for practical applications. Fifth, systematical experimental and theoretical studies on the formation

This journal is © The Royal Society of Chemistry 2021

J. Mater. Chem. A, 2021, **9**, 19534–19553 | **19549**

mechanisms of unconventional phases are desired to guide the synthesis of other unconventional phases of Au nanomaterials. Sixth, the usage of a *magic* surfactant on the crystal phase-controlled synthesis of metal nanomaterials might be extended to the synthesis of other metal nanomaterials (like Ag, Ru, Pd and Pt). This will promote the development of the emerging field of phase engineering of nanomaterials.

Last but not least, compared with Au nanocrystals obtained from other synthetic systems, the applications of Au nanomaterials synthesized from the [Au(ɪ)-oleylamine] system should be further explored. Besides catalysis and electronic devices, Au nanomaterials synthesized from [Au(ɪ)-oleylamine] may have potential applications in biology,[150–152] optics,[152,153] plasmon-enhanced spectroscopies,[27] mechanical engineering,[154] and so on. To realize these potential applications, large-scale and reproducible protocols should be developed to synthesize Au nanomaterials with a controllable size, shape and phase.

In summary, we believe this review provides useful guidance for the future development of novel Au and Au-based nanomaterials, as well as other kinds of novel inorganic nanomaterials.

Conflicts of interest

There are no conflicts to declare.

Acknowledgements

References

1 A. S. K. Hashmi and G. J. Hutchings, *Angew. Chem., Int. Ed.*, 2006, **45**, 7896–7936.

2 T. Ishida, T. Murayama, A. Taketoshi and M. Haruta, *Chem. Rev.*, 2020, **120**, 464–525.

3 L. Scarabelli, A. Sánchez-Iglesias, J. Pérez-Juste and L. M. Liz-Marzán, *J. Phys. Chem. Lett.*, 2015, **6**, 4270–4279.

4 M. Hu, J. Chen, Z.-Y. Li, L. Au, G. V. Hartland, X. Li, M. Marquez and Y. Xia, *Chem. Soc. Rev.*, 2006, **35**, 1084–1094.

5 A. A. Herzing, C. J. Kiely, A. F. Carley, P. Landon and G. J. Hutchings, *Science*, 2008, **321**, 1331–1335.

6 M. Turner, V. B. Golovko, O. P. H. Vaughan, P. Abdulkin, A. Berenguer-Murcia, M. S. Tikhov, B. F. G. Johnson and R. M. Lambert, *Nature*, 2008, **454**, 981–983.

7 S. Linic, P. Christopher and D. B. Ingram, *Nat. Mater.*, 2011, **10**, 911–921.

8 B. Zhu, S. Gong and W. Cheng, *Chem. Soc. Rev.*, 2019, **48**, 1668–1711.

9 S.-W. Lee, K.-S. Lee, J. Ahn, J.-J. Lee, M.-G. Kim and Y.-B. Shin, *ACS Nano*, 2011, **5**, 897–904.

10 C. N. Loynachan, A. P. Soleimany, J. S. Dudani, Y. Lin, A. Najer, A. Bekdemir, Q. Chen, S. N. Bhatia and M. M. Stevens, *Nat. Nanotechnol.*, 2019, **14**, 883–890.

11 M.-F. Tsai, S.-H. G. Chang, F.-Y. Cheng, V. Shanmugam, Y.-S. Cheng, C.-H. Su and C.-S. Yeh, *ACS Nano*, 2013, **7**, 5330–5342.

12 S. Diodati, P. Dolcet, M. Casarin and S. Gross, *Chem. Rev.*, 2015, **115**, 11449–11502.

13 S. K. Kulkarni, in *Nanotechnology: Principles and Practices*, Springer International Publishing, Cham, 2015, ch. 4, pp. 77–109.

14 M. Faraday, *Philos. Trans. R. Soc. London*, 1857, 145–181.

15 R. Jin, H. Qian, Z. Wu, Y. Zhu, M. Zhu, A. Mohanty and N. Garg, *J. Phys. Chem. Lett.*, 2010, **1**, 2903–2910.

16 C. S. Ah, Y. J. Yun, H. J. Park, W.-J. Kim, D. H. Ha and W. S. Yun, *Chem. Mater.*, 2005, **17**, 5558–5561.

17 Y. Kondo and K. Takayanagi, *Science*, 2000, **289**, 606–608.

18 Y. Sun and Y. Xia, *Science*, 2002, **298**, 2176–2179.

19 J. Zhang, M. R. Langille, M. L. Personick, K. Zhang, S. Li and C. A. Mirkin, *J. Am. Chem. Soc.*, 2010, **132**, 14012–14014.

20 J. Turkevich, P. C. Stevenson and J. Hillier, *Discuss. Faraday Soc.*, 1951, **11**, 55–75.

21 L. Pei, K. Mori and M. Adachi, *Langmuir*, 2004, **20**, 7837–7843.

22 S. S. Shankar, S. Bhargava and M. Sastry, *J. Nanosci. Nanotechnol.*, 2005, **5**, 1721–1727.

23 M. Brust, M. Walker, D. Bethell, D. J. Schiffrin and R. Whyman, *J. Chem. Soc., Chem. Commun.*, 1994, 801–802.

24 N. R. Jana, L. Gearheart and C. J. Murphy, *Adv. Mater.*, 2001, **13**, 1389–1393.

25 N. R. Jana, L. Gearheart and C. J. Murphy, *J. Phys. Chem. B*, 2001, **105**, 4065–4067.

26 L. Rodríguez-Lorenzo, J. M. Romo-Herrera, J. Pérez-Juste, R. A. Alvarez-Puebla and L. M. Liz-Marzán, *J. Mater. Chem.*, 2011, **21**, 11544–11549.

27 H. Chen, L. Shao, Q. Li and J. Wang, *Chem. Soc. Rev.*, 2013, **42**, 2679–2724.

28 Z. Fan, X. Huang, Y. Chen, W. Huang and H. Zhang, *Nat. Protoc.*, 2017, **12**, 2367–2376.

29 Z. Fan and H. Zhang, *Chem. Soc. Rev.*, 2016, **45**, 63–82.

30 S. Mourdikoudis and L. M. Liz-Marzán, *Chem. Mater.*, 2013, **25**, 1465–1476.

31 S. Lu, J. Liang, H. Long, H. Li, X. Zhou, Z. He, Y. Chen, H. Sun, Z. Fan and H. Zhang, *Acc. Chem. Res.*, 2020, **53**, 2106–2118.

32 Y. Chen, Z. Fan, Z. Luo, X. Liu, Z. Lai, B. Li, Y. Zong, L. Gu and H. Zhang, *Adv. Mater.*, 2017, **29**, 1701331.

33 Z. Huo, C.-k. Tsung, W. Huang, X. Zhang and P. Yang, *Nano Lett.*, 2008, **8**, 2041–2044.

34 J. Zeng, Y. Ma, U. Jeong and Y. Xia, *J. Mater. Chem.*, 2010, **20**, 2290–2301.

35 Y. Ma, J. Zeng, W. Li, M. McKiernan, Z. Xie and Y. Xia, *Adv. Mater.*, 2010, **22**, 1930–1934.

36 H. Schmidbaur and A. Schier, *Chem. Soc. Rev.*, 2012, **41**, 370–412.

37 H. You, X. Liu, H. Liu and J. Fang, *CrystEngComm*, 2016, **18**, 3934–3941.

19550 | *J. Mater. Chem. A*, 2021, **9**, 19534–19553

This journal is © The Royal Society of Chemistry 2021

38 M. B. Mohamed, K. M. AbouZeid, V. Abdelsayed, A. A. Aljarash and M. S. El-Shall, *ACS Nano*, 2010, **4**, 2766–2772.

39 Z. Fan, M. Bosman, X. Huang, D. Huang, Y. Yu, K. P. Ong, Y. A. Akimov, L. Wu, B. Li, J. Wu, Y. Huang, Q. Liu, C. Eng Png, C. Lip Gan, P. Yang and H. Zhang, *Nat. Commun.*, 2015, **6**, 7684.

40 Y. Chen, Z. Lai, X. Zhang, Z. Fan, Q. He, C. Tan and H. Zhang, *Nat. Rev. Chem.*, 2020, **4**, 243–256.

41 X. Huang, S. Li, Y. Huang, S. Wu, X. Zhou, S. Li, C. L. Gan, F. Boey, C. A. Mirkin and H. Zhang, *Nat. Commun.*, 2011, **2**, 292.

42 J. Liu, W. Niu, G. Liu, B. Chen, J. Huang, H. Cheng, D. Hu, J. Wang, Q. Liu, J. Ge, P. Yin, F. Meng, Q. Zhang, L. Gu, Q. Lu and H. Zhang, *J. Am. Chem. Soc.*, 2021, **143**, 4387–4396.

43 X. Huang, S. Li, S. Wu, Y. Huang, F. Boey, C. L. Gan and H. Zhang, *Adv. Mater.*, 2012, **24**, 979–983.

44 D. V. Leff, L. Brandt and J. R. Heath, *Langmuir*, 1996, **12**, 4723–4730.

45 H. Hiramatsu and F. E. Osterloh, *Chem. Mater.*, 2004, **16**, 2509–2511.

46 M. Aslam, L. Fu, M. Su, K. Vijayamohanan and V. P. Dravid, *J. Mater. Chem.*, 2004, **14**, 1795–1797.

47 A. Halder and N. Ravishankar, *Adv. Mater.*, 2007, **19**, 1854–1858.

48 X. Lu, M. S. Yavuz, H.-Y. Tuan, B. A. Korgel and Y. Xia, *J. Am. Chem. Soc.*, 2008, **130**, 8900–8901.

49 C. Wang, Y. Hu, C. M. Lieber and S. Sun, *J. Am. Chem. Soc.*, 2008, **130**, 8902–8903.

50 N. Pazos-Pérez, D. Baranov, S. Irsen, M. Hilgendorff, L. M. Liz-Marzán and M. Giersig, *Langmuir*, 2008, **24**, 9855–9860.

51 Z. Li, J. Tao, X. Lu, Y. Zhu and Y. Xia, *Nano Lett.*, 2008, **8**, 3052–3055.

52 A. Kisner, M. Heggen, E. Fernández, S. Lenk, D. Mayer, U. Simon, A. Offenhäusser and Y. Mourzina, *Chem.–Eur. J.*, 2011, **17**, 9503–9507.

53 R. Takahata, S. Yamazoe, K. Koyasu, K. Imura and T. Tsukuda, *J. Am. Chem. Soc.*, 2018, **140**, 6640–6647.

54 F. Pschunder, J. Puig, L. J. Giovanetti, C. Huck-Iriart, F. G. Requejo, D. Buceta, C. E. Hoppe and J. M. Ramallo-López, *J. Phys. Chem. C*, 2018, **122**, 29051–29061.

55 H. Kura and T. Ogawa, *J. Appl. Phys.*, 2010, **107**, 074310.

56 X. Huang, H. Li, S. Li, S. Wu, F. Boey, J. Ma and H. Zhang, *Angew. Chem., Int. Ed.*, 2011, **50**, 12245–12248.

57 J. A. Vargas, V. Petkov, E. S. A. Nouh, R. K. Ramamoorthy, L.-M. Lacroix, R. Poteau, G. Viau, P. Lecante and R. Arenal, *ACS Nano*, 2018, **12**, 9521–9531.

58 C. Wang, X. Li, L. Jin, P.-H. Lu, C. Dejoie, W. Zhu, Z. Wang, W. Bi, R. E. Dunin-Borkowski and K. Chen, *Nano Lett.*, 2019, **19**, 6363–6369.

59 Z. Fan, M. Bosman, Z. Huang, Y. Chen, C. Ling, L. Wu, Y. A. Akimov, R. Laskowski, B. Chen, P. Ercius, J. Zhang, X. Qi, M. H. Goh, Y. Ge, Z. Zhang, W. Niu, J. Wang, H. Zheng and H. Zhang, *Nat. Commun.*, 2020, **11**, 3293.

60 Y. Ge, Z. Huang, C. Ling, B. Chen, G. Liu, M. Zhou, J. Liu, X. Zhang, H. Cheng, G. Liu, Y. Du, C.-J. Sun, C. Tan, J. Huang, P. Yin, Z. Fan, Y. Chen, N. Yang and H. Zhang, *J. Am. Chem. Soc.*, 2020, **142**, 18971–18980.

61 P. Capdevielle, A. Lavigne, D. Sparfel, J. Baranne-Lafont, K. C. Nguyen and M. Maumy, *Tetrahedron Lett.*, 1990, **31**, 3305–3308.

62 X. Liu, M. Atwater, J. Wang, Q. Dai, J. Zou, J. P. Brennan and Q. Huo, *J. Nanosci. Nanotechnol.*, 2007, **7**, 3126–3133.

63 X. Lu, H.-Y. Tuan, B. A. Korgel and Y. Xia, *Chem.–Eur. J.*, 2008, **14**, 1584–1591.

64 J. Hrusak, R. H. Hertwig, D. Schroeder, P. Schwerdtfeger, W. Koch and H. Schwarz, *Organometallics*, 1995, **14**, 1284–1291.

65 C. Shen, C. Hui, T. Yang, C. Xiao, J. Tian, L. Bao, S. Chen, H. Ding and H. Gao, *Chem. Mater.*, 2008, **20**, 6939–6944.

66 Q. Zhang, J. Xie, Y. Yu, J. Yang and J. Y. Lee, *Small*, 2010, **6**, 523–527.

67 H. Feng, Y. Yang, Y. You, G. Li, J. Guo, T. Yu, Z. Shen, T. Wu and B. Xing, *Chem. Commun.*, 2009, 1984–1986.

68 Y. Kang, X. Ye and C. B. Murray, *Angew. Chem., Int. Ed.*, 2010, **49**, 6156–6159.

69 C. Wang, Y. Wei, H. Jiang and S. Sun, *Nano Lett.*, 2010, **10**, 2121–2125.

70 M. L. Jenkins, *Philos. Mag.*, 1972, **26**, 747–751.

71 M. Bernardi, S. N. Raja and S. K. Lim, *Nanotechnology*, 2010, **21**, 285607.

72 A. Loubat, M. Impéror-Clerc, B. Pansu, F. Meneau, B. Raquet, G. Viau and L.-M. Lacroix, *Langmuir*, 2014, **30**, 4005–4012.

73 A. Loubat, L.-M. Lacroix, A. Robert, M. Impéror-Clerc, R. Poteau, L. Maron, R. Arenal, B. Pansu and G. Viau, *J. Phys. Chem. C*, 2015, **119**, 4422–4430.

74 J. Gao, C. M. Bender and C. J. Murphy, *Langmuir*, 2003, **19**, 9065–9070.

75 R. Takahata, S. Yamazoe, K. Koyasu and T. Tsukuda, *J. Am. Chem. Soc.*, 2014, **136**, 8489–8491.

76 B. Wiley, T. Herricks, Y. Sun and Y. Xia, *Nano Lett.*, 2004, **4**, 1733–1739.

77 R. Takahata, S. Yamazoe, C. Warakulwit, J. Limtrakul and T. Tsukuda, *J. Phys. Chem. C*, 2016, **120**, 17006–17010.

78 I. Chakraborty, D. Carvalho, S. N. Shirodkar, S. Kumar, S. Bhattacharyya, R. Banerjee, U. Waghmare and P. Ayyub, *J. Phys.: Condens. Matter*, 2011, **23**, 325401.

79 H. Benaissa and M. Ferhat, *Superlattices Microstruct.*, 2017, **109**, 170–175.

80 H. Lin, J.-X. Liu, H. Fan and W.-X. Li, *J. Phys. Chem. C*, 2020, **124**, 11005–11014.

81 X. Liu, J. Luo and J. Zhu, *Nano Lett.*, 2006, **6**, 408–412.

82 C. Zhang, Y. Yao and S. Chen, *Comput. Mater. Sci.*, 2014, **82**, 372–377.

83 O. Kitakami, H. Sato, Y. Shimada, F. Sato and M. Tanaka, *Phys. Rev. B: Condens. Matter Mater. Phys.*, 1997, **56**, 13849–13854.

84 S. Illy, O. Tillement, F. Machizaud, J. M. Dubois, F. Massicot, Y. Fort and J. Ghanbaja, *Philos. Mag. A*, 1999, **79**, 1021–1031.

This journal is © The Royal Society of Chemistry 2021

J. Mater. Chem. A, 2021, **9**, 19534–19553 | **19551**

85 J. L. Huang, Z. Li, H. H. Duan, Z. Y. Cheng, Y. D. Li, J. Zhu and R. Yu, *J. Am. Chem. Soc.*, 2017, **139**, 575–578.

86 H. Schmidbaur and A. Schier, *Chem. Soc. Rev.*, 2008, **37**, 1931–1951.

87 Y. Chen, PhD thesis, Nanyang Technological University, 2018.

88 A. Janssen, Q. N. Nguyen and Y. Xia, *Angew. Chem., Int. Ed.*, 2021, **60**, 12192–12203.

89 D. Hull and D. J. Bacon, in *Introduction to Dislocations*, ed. D. Hull and D. J. Bacon, Butterworth-Heinemann, Oxford, 5th edn, 2011, ch. 1, pp. 1–20.

90 A. T. Krawczynska, M. Kerber, P. Suchecki, B. Romelczyk-Baishya, M. Lewandowska and D. Setman, *Mater. Sci. Eng. A*, 2021, **808**, 140913.

91 T. Tan, S. Zhang, J. Wang, Y. Zheng, H. Lai, J. Liu, F. Qin and C. Wang, *Nanoscale*, 2021, **13**, 195–205.

92 S. D. Golze, R. A. Hughes, S. Rouvimov, R. D. Neal, T. B. Demille and S. Neretina, *Nano Lett.*, 2019, **19**, 5653–5660.

93 Y. Yu, F. Cui, J. Sun and P. Yang, *Nano Lett.*, 2016, **16**, 3078–3084.

94 D. A. Moraes, J. B. S. Junior, F. F. Ferreira, N. V. V. Mogili and L. C. Varanda, *Nanoscale*, 2020, **12**, 13316–13329.

95 Q. Zhang, N. Li, J. Goebl, Z. Lu and Y. Yin, *J. Am. Chem. Soc.*, 2011, **133**, 18931–18939.

96 Y. Xiong and Y. Xia, *Adv. Mater.*, 2007, **19**, 3385–3391.

97 Y. Zheng, J. Zeng, A. Ruditskiy, M. Liu and Y. Xia, *Chem. Mater.*, 2014, **26**, 22–33.

98 Y. Xia, Y. Xiong, B. Lim and S. E. Skrabalak, *Angew. Chem., Int. Ed.*, 2009, **48**, 60–103.

99 J. Chen, T. Herricks and Y. Xia, *Angew. Chem., Int. Ed.*, 2005, **44**, 2589–2592.

100 Y. Xiong, J. M. McLellan, J. Chen, Y. Yin, Z.-Y. Li and Y. Xia, *J. Am. Chem. Soc.*, 2005, **127**, 17118–17127.

101 V. Germain, J. Li, D. Ingert, Z. Wang and M. Pileni, *J. Phys. Chem. B*, 2003, **107**, 8717–8720.

102 Z. Guo, Y. Zhang, A. Xu, M. Wang, L. Huang, K. Xu and N. Gu, *J. Phys. Chem. C*, 2008, **112**, 12638–12645.

103 D. Seo, C. I. Yoo, I. S. Chung, S. M. Park, S. Ryu and H. Song, *J. Phys. Chem. C*, 2008, **112**, 2469–2475.

104 R. Long, S. Zhou, B. J. Wiley and Y. Xiong, *Chem. Soc. Rev.*, 2014, **43**, 6288–6310.

105 I. Markov and S. Stoyanov, *Contemp. Phys.*, 1987, **28**, 267–320.

106 F.-R. Fan, D.-Y. Liu, Y.-F. Wu, S. Duan, Z.-X. Xie, Z.-Y. Jiang and Z.-Q. Tian, *J. Am. Chem. Soc.*, 2008, **130**, 6949–6951.

107 C. Tan, J. Chen, X.-J. Wu and H. Zhang, *Nat. Rev. Mater.*, 2018, **3**, 17089.

108 Y. Xia, K. D. Gilroy, H. C. Peng and X. Xia, *Angew. Chem., Int. Ed.*, 2017, **56**, 60–95.

109 M. Zhao and Y. Xia, *Nat. Rev. Mater.*, 2020, **5**, 440–459.

110 K. D. Gilroy, X. Yang, S. Xie, M. Zhao, D. Qin and Y. Xia, *Adv. Mater.*, 2018, **30**, 1706312.

111 Y. Chen, Z. Fan, J. Wang, C. Ling, W. Niu, Z. Huang, G. Liu, B. Chen, Z. Lai and X. Liu, *J. Am. Chem. Soc.*, 2020, **142**, 12760–12766.

112 M. Zhao, L. Xu, M. Vara, A. O. Elnabawy, K. D. Gilroy, Z. D. Hood, S. Zhou, L. Figueroa-Cosme, M. Chi and M. Mavrikakis, *ACS Catal.*, 2018, **8**, 6948–6960.

113 L. Gloag, T. M. Benedetti, S. Cheong, C. E. Marjo, J. J. Gooding and R. D. Tilley, *J. Am. Chem. Soc.*, 2018, **140**, 12760–12764.

114 A. P. LaGrow, S. Cheong, J. Watt, B. Ingham, M. F. Toney, D. A. Jefferson and R. D. Tilley, *Adv. Mater.*, 2013, **25**, 1552–1556.

115 L. Onsager, *Ann. N. Y. Acad. Sci.*, 1949, **51**, 627–659.

116 L. Zhang, Z.-J. Zhao and J. Gong, *Angew. Chem., Int. Ed.*, 2017, **56**, 11326–11353.

117 J. Wu, T. Sharifi, Y. Gao, T. Zhang and P. M. Ajayan, *Adv. Mater.*, 2019, **31**, 1804257.

118 Y. Wang, P. Han, X. Lv, L. Zhang and G. Zheng, *Joule*, 2018, **2**, 2551–2582.

119 Y. Yang, Y. Zhang, J.-S. Hu and L.-J. Wan, *Acta Phys. -Chim. Sin.*, 2020, **36**, 1906085.

120 T. Cheng, Y. Huang, H. Xiao and W. A. Goddard, *J. Phys. Chem. Lett.*, 2017, **8**, 3317–3320.

121 H. Mistry, A. S. Varela, S. Kühl, P. Strasser and B. R. Cuenya, *Nat. Rev. Mater.*, 2016, **1**, 16009.

122 W. Zhu, R. Michalsky, O. Metin, H. Lv, S. Guo, C. J. Wright, X. Sun, A. A. Peterson and S. Sun, *J. Am. Chem. Soc.*, 2013, **135**, 16833–16836.

123 W. Zhu, Y. J. Zhang, H. Zhang, H. Lv, Q. Li, R. Michalsky, A. A. Peterson and S. Sun, *J. Am. Chem. Soc.*, 2014, **136**, 16132–16135.

124 Y. Wang, C. Li, Z. Fan, Y. Chen, X. Li, L. Cao, C. Wang, L. Wang, D. Su, H. Zhang, T. Mueller and C. Wang, *Nano Lett.*, 2020, **20**, 8074–8080.

125 M. Gao, Y. Zhu, Y. Liu, K. Wu, H. Lu, S. Tang, C. Liu, H. Yue, B. Liang and J. Yan, *Chem. Commun.*, 2020, **56**, 7021–7024.

126 X. X. Wang, M. T. Swihart and G. Wu, *Nat. Catal.*, 2019, **2**, 578–589.

127 D. Banham and S. Ye, *ACS Energy Lett.*, 2017, **2**, 629–638.

128 Y. Lee, A. Loew and S. Sun, *Chem. Mater.*, 2010, **22**, 755–761.

129 C. Tang and S.-Z. Qiao, *Chem. Soc. Rev.*, 2019, **48**, 3166–3180.

130 X. Cui, C. Tang and Q. Zhang, *Adv. Energy Mater.*, 2018, **8**, 1800369.

131 C. Chen, C. Liang, J. Xu, J. Wei, X. Li, Y. Zheng, J. Li, H. Tang and J. Li, *Electrochim. Acta*, 2020, **335**, 135708.

132 S. Dey and G. C. Dhal, *Mater. Today Chem.*, 2019, **14**, 100180.

133 N. K. Soliman, *J. Mater. Res. Technol.*, 2019, **8**, 2395–2407.

134 S. Peng, Y. Lee, C. Wang, H. Yin, S. Dai and S. Sun, *Nano Res.*, 2008, **1**, 229–234.

135 C. Xu, P. Ravi Anusuyadevi, C. Aymonier, R. Luque and S. Marre, *Chem. Soc. Rev.*, 2019, **48**, 3868–3902.

136 Z. Zhang, C. Zhang, H. Zheng and H. Xu, *Acc. Chem. Res.*, 2019, **52**, 2506–2515.

137 J. Long, H. Chang, Q. Gu, J. Xu, L. Fan, S. Wang, Y. Zhou, W. Wei, L. Huang, X. Wang, P. Liu and W. Huang, *Energy Environ. Sci.*, 2014, **7**, 973–977.

19552 | *J. Mater. Chem. A*, 2021, **9**, 19534–19553

This journal is © The Royal Society of Chemistry 2021

138 J. Huang, W. Niu, C. Li, C. Tan, P. Yin, H. Cheng, Z. Hu, N. Yang, Q. He, G.-H. Nam and H. Zhang, *ACS Mater. Lett.*, 2020, **2**, 409–414.

139 S. Gong and W. Cheng, *Adv. Electron. Mater.*, 2017, **3**, 1600314.

140 J. H. M. Maurer, L. González-García, B. Reiser, I. Kanelidis and T. Kraus, *Nano Lett.*, 2016, **16**, 2921–2925.

141 Y. Chen, Z. Ouyang, M. Gu and W. Cheng, *Adv. Mater.*, 2013, **25**, 80–85.

142 S. Gong, Y. Zhao, L. W. Yap, Q. Shi, Y. Wang, J. A. P. B. Bay, D. T. H. Lai, H. Uddin and W. Cheng, *Adv. Electron. Mater.*, 2016, **2**, 1600121.

143 Q. Zhai, Y. Liu, R. Wang, Y. Wang, Q. Lyu, S. Gong, J. Wang, G. P. Simon and W. Cheng, *Adv. Energy Mater.*, 2020, **10**, 1903512.

144 S. Gong, S. Du, J. Kong, Q. Zhai, F. Lin, S. Liu, N. R. Cameron and W. Cheng, *Small*, 2020, **16**, 2003269.

145 S. Kundu, A. Leelavathi, G. Madras and N. Ravishankar, *Langmuir*, 2014, **30**, 12690–12695.

146 S. Gong, W. Schwalb, Y. Wang, Y. Chen, Y. Tang, J. Si, B. Shirinzadeh and W. Cheng, *Nat. Commun.*, 2014, **5**, 3132.

147 S. Gong, D. T. H. Lai, B. Su, K. J. Si, Z. Ma, L. W. Yap, P. Guo and W. Cheng, *Adv. Electron. Mater.*, 2015, **1**, 1400063.

148 S. Gong, D. T. H. Lai, Y. Wang, L. W. Yap, K. J. Si, Q. Shi, N. N. Jason, T. Sridhar, H. Uddin and W. Cheng, *ACS Appl. Mater. Interfaces*, 2015, **7**, 19700–19708.

149 W. Niu, J. Liu, J. Huang, B. Chen, Q. He, A.-L. Wang, Q. Lu, Y. Chen, Q. Yun, J. Wang, C. Li, Y. Huang, Z. Lai, Z. Fan, X.-J. Wu and H. Zhang, *Nat. Commun.*, 2019, **10**, 2881.

150 M.-C. Daniel and D. Astruc, *Chem. Rev.*, 2004, **104**, 293–346.

151 E. C. Dreaden, A. M. Alkilany, X. Huang, C. J. Murphy and M. A. El-Sayed, *Chem. Soc. Rev.*, 2012, **41**, 2740–2779.

152 N. Li, P. Zhao and D. Astruc, *Angew. Chem., Int. Ed.*, 2014, **53**, 1756–1789.

153 Y. Ni, C. Kan, J. Xu and Y. Liu, *Superlattices Microstruct.*, 2018, **114**, 124–142.

154 J. Wang, F. Sansoz, J. Huang, Y. Liu, S. Sun, Z. Zhang and S. X. Mao, *Nat. Commun.*, 2013, **4**, 1742.

This journal is © The Royal Society of Chemistry 2021

J. Mater. Chem. A, 2021, **9**, 19534–19553 | **19553**